Theses and Dissertations   1. Thesis and Dissertation Collection, all items

1997-06

Final design, integration and validation of the PANSAT antenna system

Smilowitz, Gary J

Monterey, California. Naval Postgraduate School

http://hdl.handle.net/10945/8407

NAVAL POSTGRADUATE SCHOOL
MONTEREY, CALIFORNIA

THESIS

FINAL DESIGN, INTEGRATION AND VALIDATION OF THE PANSAT ANTENNA SYSTEM

by

Gary J. Smilowitz

June, 1997

Thesis Advisor: Richard W. Adler

Approved for public release; distribution is unlimited.

REPORT DOCUMENTATION PAGE		Form Approved OMB No. 0704-0188

Public reporting burden for this collection of information is estimated to average 1 hour per response, including the time for reviewing instruction, searching existing data sources, gathering and maintaining the data needed, and completing and reviewing the collection of information. Send comments regarding this burden estimate or any other aspect of this collection of information, including suggestions for reducing this burden, to Washington Headquarters Services, Directorate for Information Operations and Reports, 1215 Jefferson Davis Highway, Suite 1204, Arlington, VA 22202-4302, and to the Office of Management and Budget, Paperwork Reduction Project (0704-0188) Washington DC 20503.

1. AGENCY USE ONLY *(Leave blank)*	2. REPORT DATE 19 June 1997.	3. REPORT TYPE AND DATES COVERED Master's Thesis	
4. TITLE AND SUBTITLE **FINAL DESIGN, INTEGRATION AND VALIDATION OF THE PANSAT ANTENNA SYSTEM**		5. FUNDING NUMBERS	
6. AUTHOR(S) Gary J. Smilowitz			
7. PERFORMING ORGANIZATION NAME(S) AND ADDRESS(ES) Naval Postgraduate School Monterey CA 93943-5000		8. PERFORMING ORGANIZATION REPORT NUMBER	
9. SPONSORING/MONITORING AGENCY NAME(S) AND ADDRESS(ES)		10. SPONSORING/MONITORING AGENCY REPORT NUMBER	
11. SUPPLEMENTARY NOTES The views expressed in this thesis are those of the author and do not reflect the official policy or position of the Department of Defense or the U.S. Government.			
12a. DISTRIBUTION/AVAILABILITY STATEMENT Approved for public release; distribution is unlimited.		12b. DISTRIBUTION CODE	

13. ABSTRACT *(maximum 200 words)*

   In this thesis, the final design for the Petite Amateur Navy Satellite (PANSAT) antenna system is constructed, integrated and validated. The antenna elements and matching network are field tested and compared to the Numerical Electromagnetics Code (NEC) model. The final free-space radiation pattern and its power gain distribution will be used to help track PANSAT's rotation during its orbit.

14. SUBJECT TERMS Satellite Antenna Design Numerical Electromagnetics Code (NEC) PANSAT				15. NUMBER OF PAGES 87
				16. PRICE CODE
17. SECURITY CLASSIFICATION OF REPORT Unclassified	18. SECURITY CLASSIFICATION OF THIS PAGE Unclassified	19. SECURITY CLASSIFICATION OF ABSTRACT Unclassified	20. LIMITATION OF ABSTRACT UL	

NSN 7540-01-280-5500

FINAL DESIGN, INTEGRATION AND VALIDATION OF THE PANSAT ANTENNA SYSTEM

Gary J. Smilowitz
Lieutenant Commander, United States Navy
B.E. EE, Vanderbilt University, 1985

Submitted in partial fulfillment
of the requirements for the degree of

MASTER OF SCIENCE IN ELECTRICAL ENGINEERING

from the

NAVAL POSTGRADUATE SCHOOL
June 1997

ABSTRACT

In this thesis, the final design for the Petite Amateur Navy Satellite (PANSAT) antenna system is constructed, integrated and validated. The antenna elements and matching network are field tested and compared to the Numerical Electromagnetics Code (NEC) model. The final free-space radiation pattern and its power gain distribution will be used to help track PANSAT's rotation during its orbit.

TABLE OF CONTENTS

LIST OF FIGURES

LIST OF SYMBOLS

λ Wavelength

θ Angle from +Z axis

ϕ Angle from +X axis

c   Velocity of Light (3×10^8 m /s)

f   Frequency (Hz)

θ_{rot} Rotation Angle of PANSAT from vertical position

ϕ_{rot} Rotation of PANSAT from direct line of Receiver

θ_{sat} Satellite Body fixed angle from +Z axis

ϕ_{sat} Satellite Body fixed azimuth angle from +X axis

ACKNOWLEDGEMENTS

Numerous individuals assisted me in completing this thesis by providing advice, encouragement, and technical expertise. I'm indeed grateful for all their invaluable contributions.

Of those who helped me, a few deserve special mention. **Professor Adler** provided the technical expertise and supervision I needed to complete this project. I will always appreciate his patience and clarity.

The entire **SSAG PANSAT Engineering Staff** for including me in their project as an equal. I have to especially thank **David Rigmaiden** , who acted as my mentor throughout this entire project. He helped me to focus my imagination, and gave me the courage to explore all possibilities. He was an excellent teacher, and I'll always be grateful.

I also want to thank **Professor Panholzer** for allowing me to combine my academic experience at the Naval Postgraduate School with a truly fascinating and fun project.

Finally, I want to thank my beautiful, funny wife **Margie**. She always provided strength, encouragement, and devotion and kept me focused throughout all my studies. I could not have finished without her.

I.   INTRODUCTION

A.   OBJECTIVES

The objective of this thesis is to validate the final design of the Petite Amateur Navy Satellite (PANSAT) antenna system. The previous thesis by Ercument Karipinar, June 1995, used the Numerical Electromagnetics Code (NEC) to model PANSAT and recommended an "optimum configuration" [Ref. 1] for the antenna system.

This thesis completes that effort with the actual construction and testing of that design. In addition to NEC, individual antenna elements, the matching network, and a working scale model of PANSAT were used.

The final radiation pattern and its associated power gains will be utilized by the ground station to help monitor PANSAT's rotation during its orbit.

B.   PANSAT SPECIFICATIONS

PANSAT is a small, lightweight, tumbling communications satellite that will provide low earth coverage for approximately two years within the amateur radio frequency band. Its primary mission is to expose Naval Postgraduate School (NPS) students to the complete design and operation of a communications satellite. PANSAT will also provide a store-and-forward communications ability for amateur radio operators around the world and will illustrate the potential of miniature and micro-satellites.   This innovative project is supported by a cadre of full time engineers employed by the Space Systems Academic Group at NPS. They have been supplemented, since its inception in 1989, by many NPS thesis students who will continue this effort as PANSAT nears its final preparations and tests for launch. Figure 1 is an excellent picture of the spacecraft with the antennas attached.

The satellite is a 150 pound, 19 inch diameter, 26 sided polyhedron designed for launch as a space shuttle secondary payload. It will be jettisoned using the Get Away Special (GAS) canister under the Hitchhiker program.
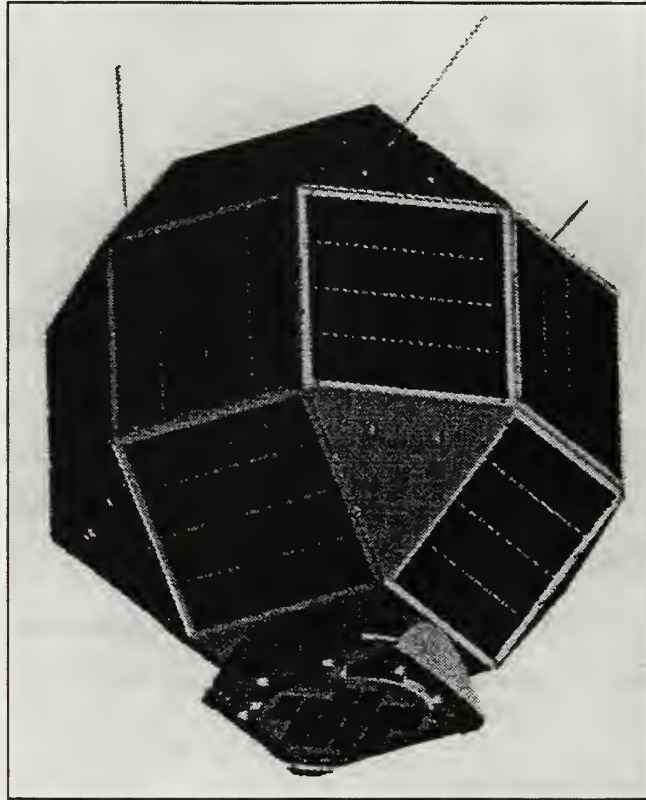
Figure 1 PANSAT with antennas and initial Launch Vehicle Interface (LVI)

The spacecraft is constructed of 6061-T6 aluminum and is treated on all parts (with the exception of the battery box) with a chemical finish which ensures uniform electrical conduction. Sixteen silicon solar panels will be attached to the square sections of the spacecraft while a more efficient GaAs solar panel will be attached to the bottom of the circular Launch Vehicle Interface (LVI). This arrangement provides the necessary power as the spacecraft freely tumbles in its orbit. The lower four triangular sections will not have any solar cells attached to them.

PANSAT has a direct sequence spread spectrum (DSSS), differentially encoded binary phase shift-keyed (DBPSK) communications system. The center frequency is 436.5 MHz with a chip rate of 1.25 MHz and a code length of 127 chips. These lead to a bit rate of 9,842 bps. As described in Karipinar's thesis [Ref. 2], this system is resistant to interference and difficult to jam. It will be able to store up to 4 MB of memory, and send and receive messages as it passes overhead. Figure 2 on page 3 shows an expanded view of PANSAT and its subsystems.

Antennas (4)

Solar Panels (5)

Mass Storage (9 MB)

Analog Muxing

Upper Equipment Platform

Solar Panels (8)

Electric Power Subsystem (EPS)

Digital Control Subsystem (DCS)

Lower Equipment Platform

Battery Box (2)

Support Cylinder

Communication Subsystem (RF)

Baseplate

Solar Panels (4)

Launch Vehicle Interface (LVI)

Solar Panel

Microswitches (3)
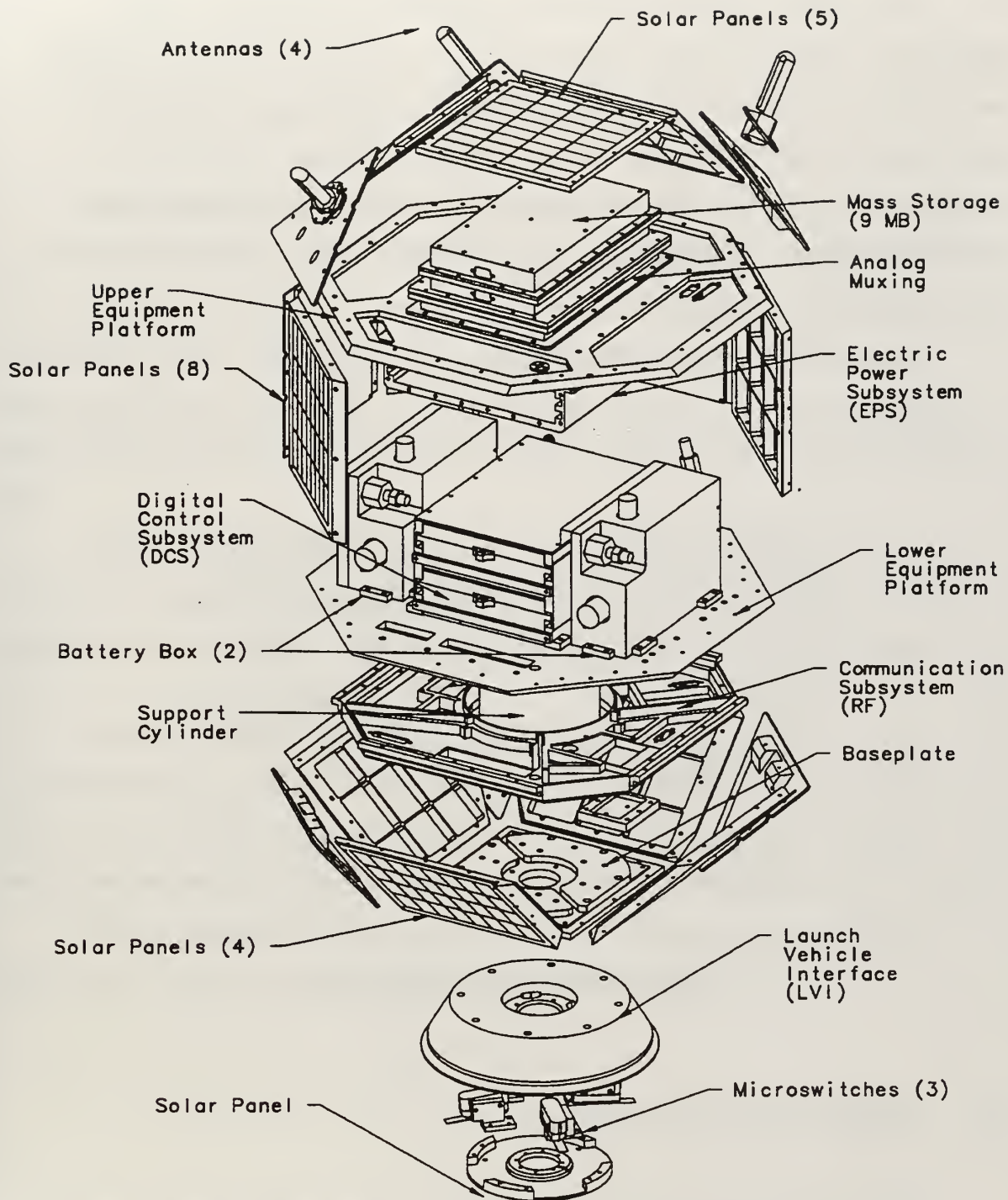
Figure 2 Expanded Subsystem View from PANSAT documents

3

C. PREVIOUS ANTENNA DEVELOPMENT

The original design, based on previous research by Daniel Ellrick in 1991, determined a tangential turnstile configuration would satisfy the coverage specifications and possible polarization problems due to the satellite's tumbling [Ref. 1]. The optimum configuration for the antenna placement was finalized in Karipinar's thesis [Ref. 2]. It was estimated using NEC, that the antennas should be placed "on the upper triangles, bisecting the triangle and centered. The orientation angles are $\theta = 45^0$ (distance from +Z) and $\phi = 0,90,180$, and 270" [Ref. 2].

Figure 3 shows this final configuration.

Side View   Top View
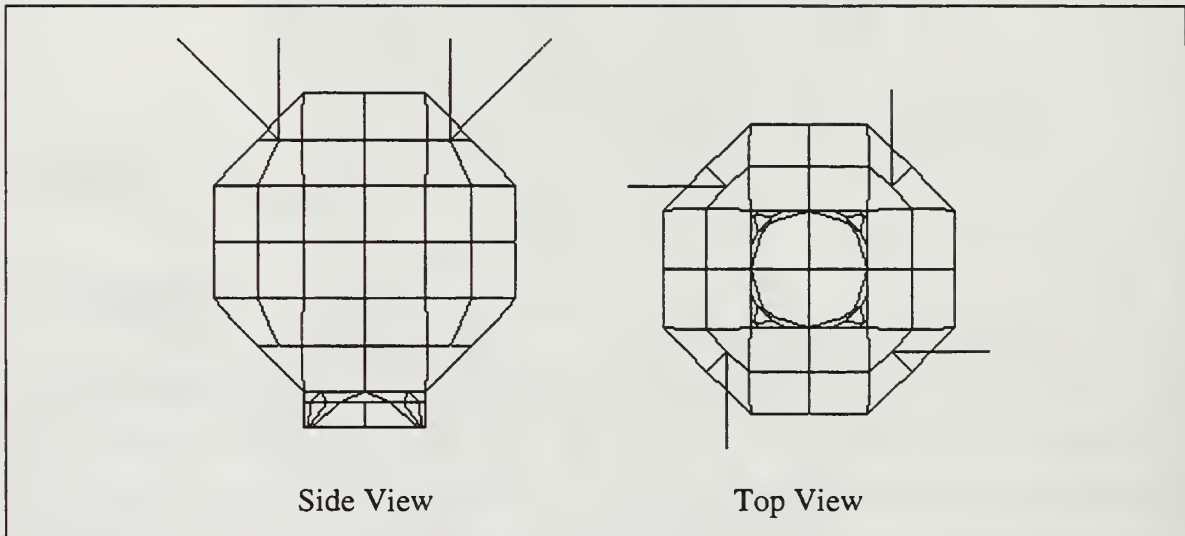
Figure 3 Final Antenna Placement

D. DESIGN AND TESTING PLAN

The antenna system was tested and validated at certain stages of the development. The following steps show the approach taken to develop the test plan, and was used as a guide throughout this research:

1. Final Antenna Design

2. Test New vs. Original Designs

3. Test Matching Network

4. Integrate and Field Test

5. Final Comparison of Field vs. NEC Simulation.

The initial task for this thesis was to construct the antenna element so that its basic properties (length, width, impedance) were very close to the theoretical design. This process is discussed in Chapter II. Next, the old and new designs had to be physically tested and compared to one another. This was accomplished by exciting each antenna design separately over a simulated (25' x 25') infinite ground plane. By comparing their characteristic impedances, a judgment could be made whether or not this new design was valid.

Parallel with the antenna tests, the feed system was designed and tested. The primary goal of this network is to match the final antenna system impedance to the $50\,\Omega$ impedance of the rf circuit. The detailed description of this process is found in Chapter III.

After both the antenna elements and the feed system satisfied the initial design tests, they were integrated onto a scale model of PANSAT made from wood and heavy aluminum foil. This model was then field tested (as described in Chapter IV) and the data compared to the NEC model designed to match the field's environment.

When the testing was complete, conclusions were then made whether the free-space model by NEC was sufficient for use in future modeling and data.

II.   ELEMENT DESIGN

A.   ANTENNA SPECIFICATIONS

The antenna elements needed to satisfy the following conditions:

1. PANSAT must fit into a GAS canister, unimpeded by antennas.
2. Once deployed, the antenna blades must be rigid enough to remain extended.
3. Antenna-mount assembly must be simple for repeated construction.
4. Must be easily attached and removed if required.

The antenna elements, once integrated onto PANSAT, must fit within the GAS canister for the pre-launch configuration. The clearance between the spacecraft and the interior of this canister is only 0.5 inches. This setup is shown in Figure 4.
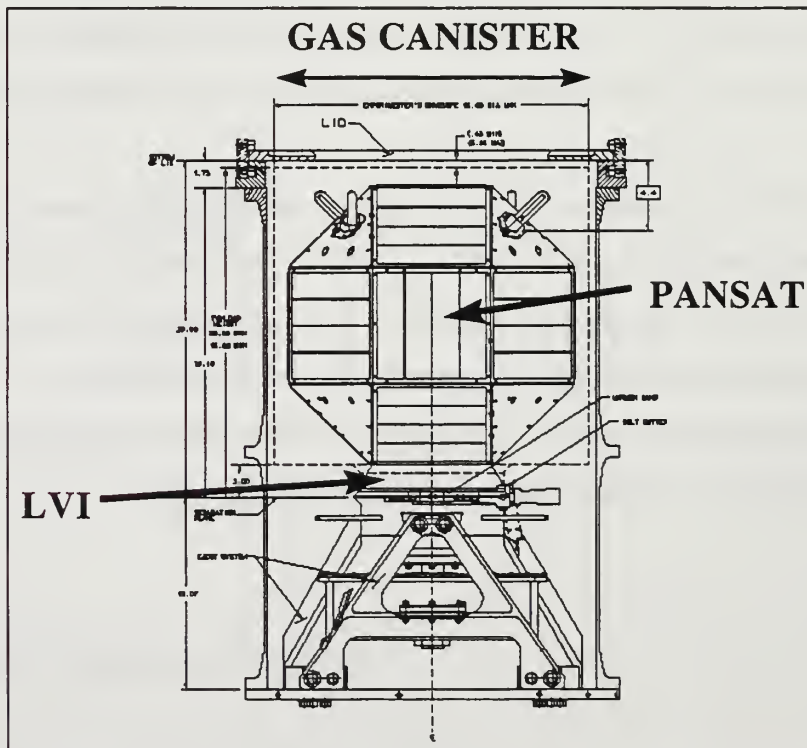
Figure 4 PANSAT within GAS (Pre-launch)

Therefore, the original design had to be changed from a rod whose length was $\lambda/4$ (17 cm) with radius .0045m to a shape that could be folded and stowed easily within this container. A flat strip was chosen for its obvious flexibility, and its width was calculated using the following conversion [Ref. 3]:

$$a = d/4$$

Where **a** is the radius of the tube and **d** is the width of the strip. This calculation resulted in a width of **18mm**. It was decided that the material for the antenna blades would be beryllium-copper. This would satisfy the necessity for both good conductance and rigidity. The bottom end of the antenna blade is tapered to a point to allow for even distribution of current from the SMA connector. This end is then soldered to the connector to provide both the contact and mechanical support. Figure 5 illustrates this arrangement.
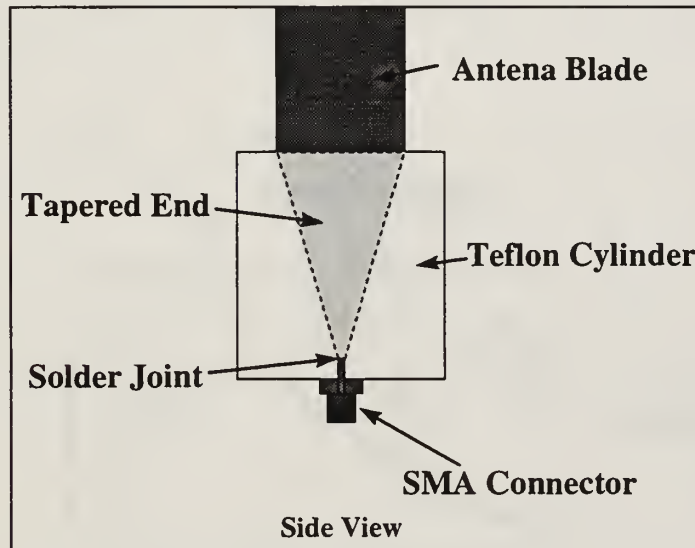
Figure 5 Internal View of Tapered Blade

The support for the antenna blade needs to provide the added rigidity after the blade has extended after deployment. This was accomplished by fitting the bottom of the blade between a teflon tube and cylinder. This small radius at the one end of the antenna provides the extension support required.

This unit (the antenna and teflon cylinder) was then placed inside (very tight fit) an aluminum cup that would later be milled in one piece with the antenna clamp. This assembly, already at the proper angles required for the antenna, is then attached to the triangular antenna plate on the spacecraft.

The antenna's SMA connector protrudes from the bottom of the cup for attachment to the matching network. The antenna clamp (cup and attachment collar) allows for full electrical contact of the spacecraft around the antenna to act as the ground plane. The final design configuration is shown in Figure 6. This final assembly allows for quick attachment and removal of the antenna element if required. It is also easily assembled requiring only one solder joint (blade and SMA connector).
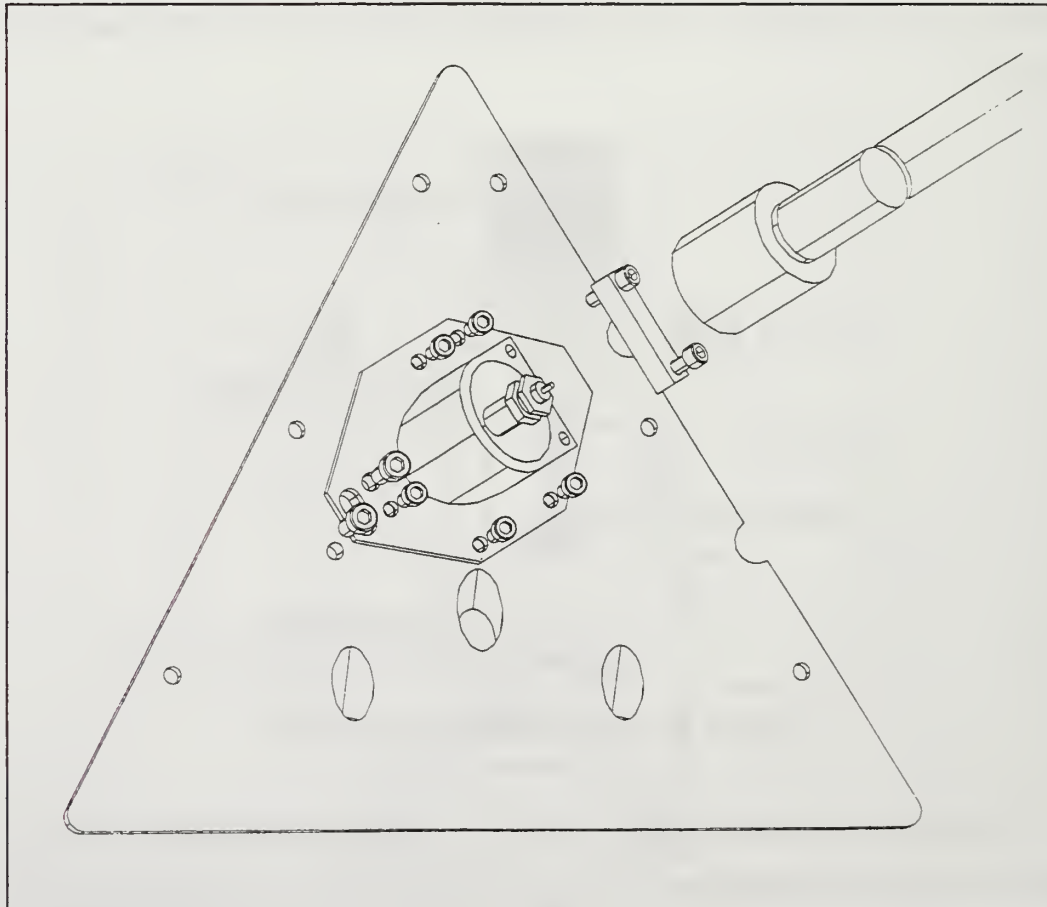
Figure 6 Antenna and Adapter Cup

B.   TESTING AND MODELING

The primary concern at this point in the design is whether the new blade antenna is a valid physical representation of the theoretical model used in the previous research. To compare their characteristics, a rod antenna was built using the same radius as in the model, and both elements were tested separately over a ground plane.

This plane was considered "infinite" as its size was much larger than a wavelength. Values for impedance and Standing Wave Ratio (SWR) were observed using an HP 4396A Network Analyzer and an HP 85046A S-Parameter test set. The lengths of the elements were decreased and the frequencies 435, 436.5 and 438 MHz were sampled. The impedance difference between the two elements at the center frequency for a length of quarter wavelength (6.7 in.) was approximately 7 Ω. This satisfied the comparison of the blade and theoretical elements. The SWR for the new blade element was 1.42 at the center frequency. The impedance comparisons (436.5 MHz only) are shown in Figure 7.
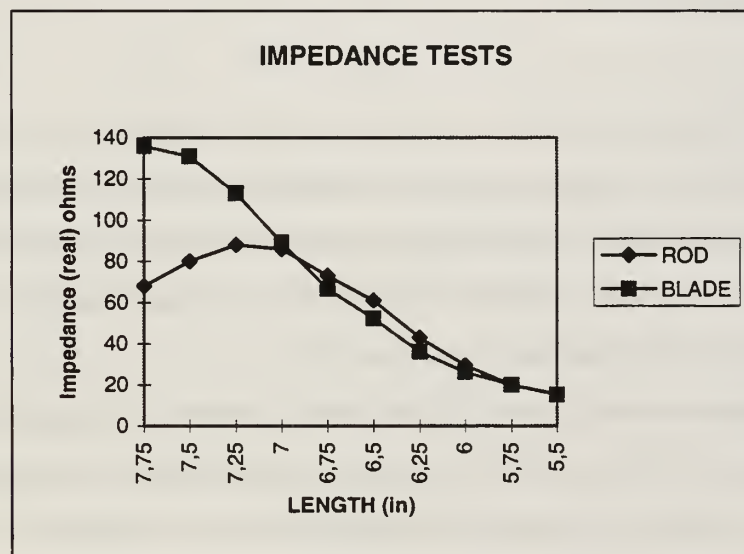
Figure 7 Ground Plane Test

The final impedance measurements of the ground plane test were then matched in the NEC model and compared to the tested results using a Smith chart. This model was then added to the original PANSAT NEC model and run as the final configuration. Figure 8 shows this antenna modeled over the ground plane.
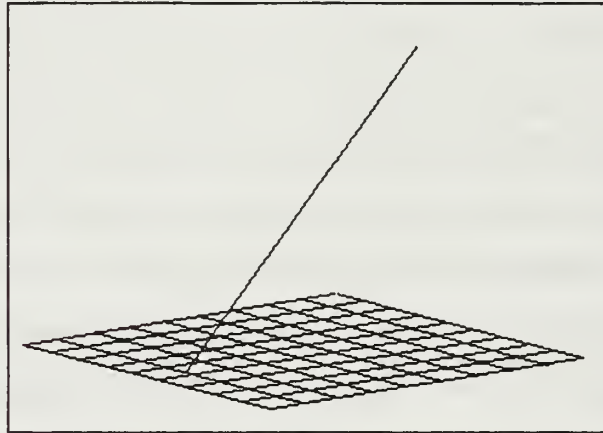
Figure 8 Modeled Antenna over Ground Plane

C.   INTEGRATION

The final design for the antenna element was now verified using both physical field testing over the ground plane, and NEC modeling. Four new elements and their mounts were then constructed. For this design stage only, the blades were hand-rolled to establish an initial bend in the elements. Procedures for automatic bending with sufficient curvature of the blade are being developed.

The triangular antenna plates along with the new antennas clamped into position were attached to the PANSAT scale model for the final field tests. The method of connecting these antennas to the matching network will be discussed in the Chapter III .

III.   ANTENNA FEED SYSTEM

A.   SPECIFICATIONS AND DESIGN

The antenna feed system will connect PANSAT's transponder circuitry to the antenna configuration. The basic requirements for this network are:

1. The phase quadrature must be maintained.
2. The power must be divided equally among the antennas.
3. The impedance seen at the matching network's input should be close to the 50 Ω rf network impedance (The SWR should be 1.4 or lower).

The tangential turnstile antenna system is designed to utilize a 90° phase change with each antenna, resulting in 360° total coverage. This phase division must be accompanied by an equal power split among the antenna elements to ensure a symmetric radiation pattern. These two requirements were satisfied by using two types of dividers within the feed network.

The signal from the rf section of the satellite is first fed into a 180° power/phase divider which results in a 3 dB drop and two separate signals. These new signals are then input to a quadrature hybrid divider, which will evenly split the power and shift the phase of each signal by 90°. This results in four separate signals, each with a 6 dB power drop from the original input, and a 90° progressive phase shift from element to element. Figure 9 on page 12 shows a block diagram of this matching network.

The requirement for the input of this matching network to be 50 Ω is satisfied by the properties of the quadrature hybrid dividers. By connecting identical antenna elements to the two output ports of the quad-hybrid, slight phase differences are routed to a terminated port. This ensures that the SWR seen at the input of the device is the reflection from the antenna impedance differences and not individual element phase changes due to imperfections. The manufacturer claims that these devices will perform for element impedances of up to 110 Ω each.

11

The four antenna elements with their teflon supports were attached to antenna clamps using identical methods. Slight differences in individual impedances may occur, but they would be minimal at worst.
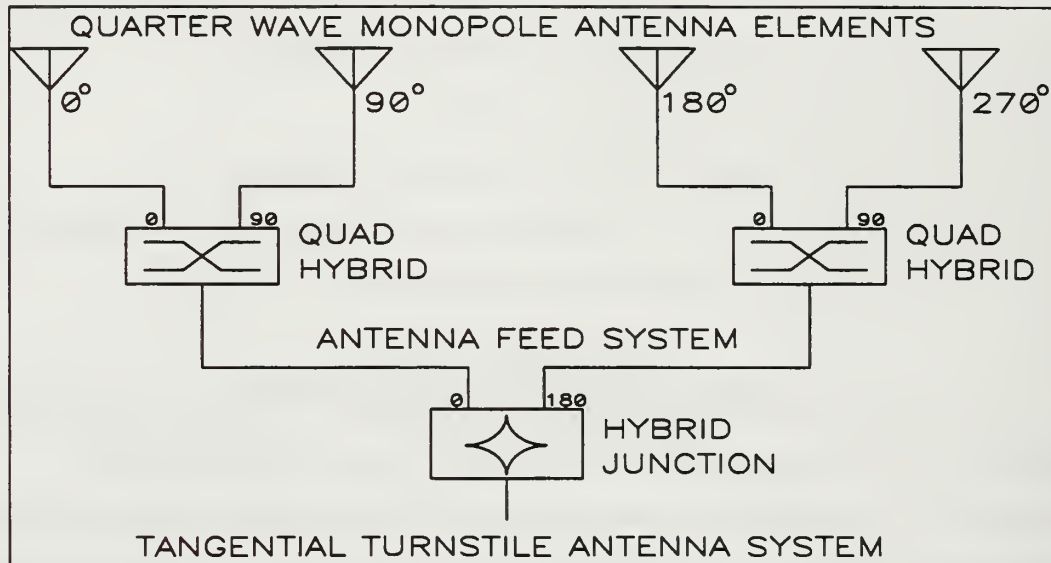
Figure 9 Matching Network

B. TESTING

The two validating criteria for the matching network were the phase differences between the four antenna ports and the power output to each of the elements at their SMA connectors.

This was accomplished by first sampling the matching network at the four output SMA connectors. If the tests were satisfactory, identical coaxial cables were then attached and sampled at their ends to ensure the proper phase shift. Table 1 and Table 2 show the results of these tests. Figure 10 and Figure 11 are polar representations.

The polar plots both indicate a successful phase progression at the four output ports, with and without the coaxial cables attached. The power outputs, ranging from -7.5 to -8.1 dB, are also within specifications considering the small losses due to the circuitry and line loss.

NETWORK PORT	PHASE (degrees)	POWER OUTPUT (dB)
1	-67	-7.5
2	14	-7.5
3	109	-7.5
4	-168	-7.8

Table 1 Matching Network Test without Coax
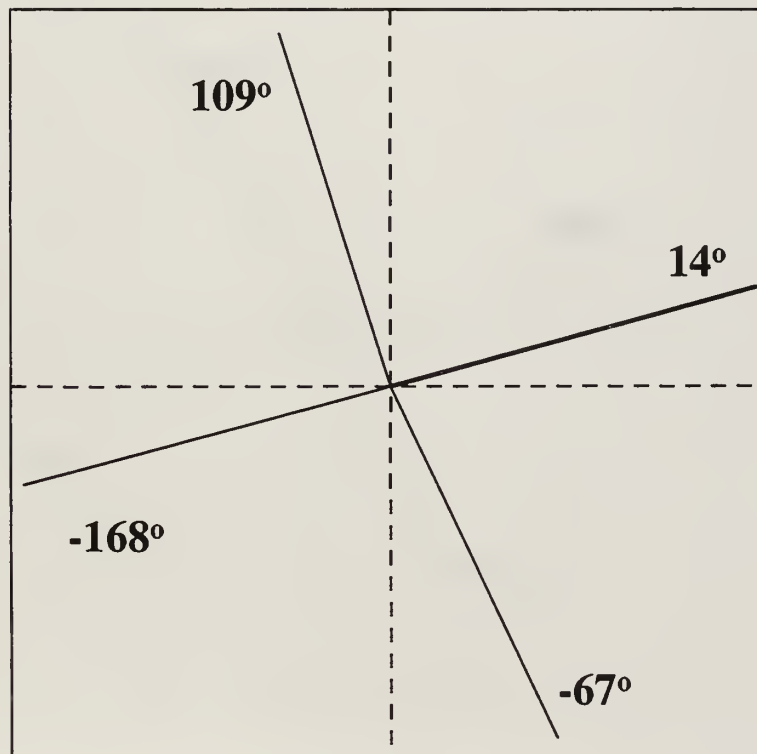
Figure 10 Polar Plot of Table 1

13

NETWORK PORT	PHASE (degrees)	POWER OUTPUT (dB)
1	163	-8.1
2	-117.5	-7.9
3	-22	-7.8
4	60	-8.8

Table 2 Matching Network Test with Coax Cable
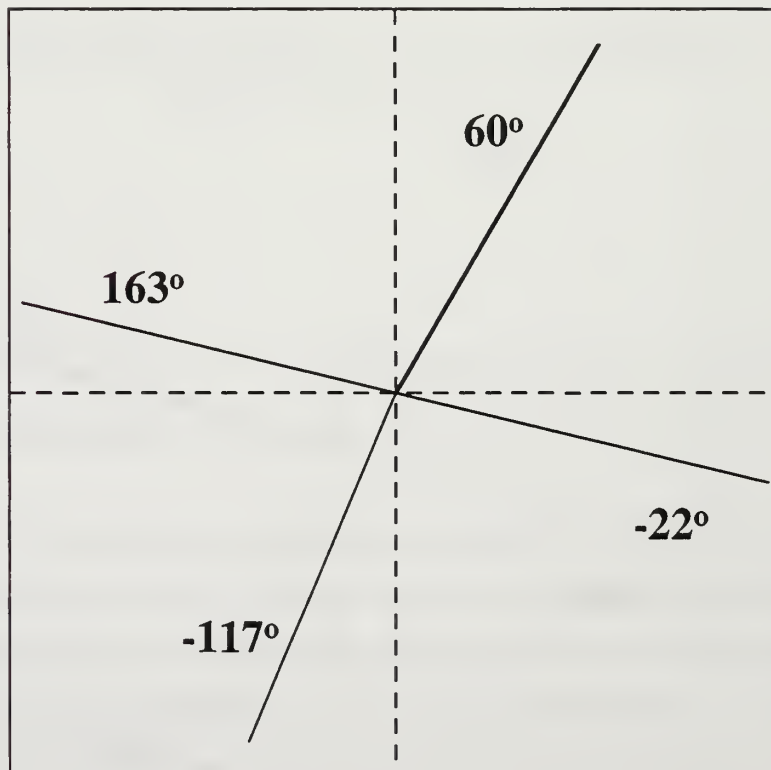
Figure 11 Polar Plot of Table 2

14

C.   INTEGRATION

The validated matching network was now integrated into the total antenna system on the scale model of PANSAT by attaching the coaxial cables from the output ports of the feed network to each of the input SMA connectors of the antenna assembly. These output ports were renumbered (1 through 4) according to the final relative phase positions shown in Figure 11. This insured that the phase difference between each monopole would be 90°, and therefore result in 360° of total coverage.

The matching network was placed inside the PANSAT model on the top shelf (where the base of the triangular plates begin) and a hole drilled through to allow the input cable from the signal oscillator (simulating the rf section) to be fed.   The final configuration for field testing is discussed in Chapter IV.

IV. FINAL DESIGN

A. FIELD TESTS

The previous research determined the optimum configuration for the antenna elements on PANSAT. This design produced a symmetrical radiation pattern that could be tracked and utilized by the ground station in the future. The free-space radiation pattern as modeled in NEC is shown in Figure 12.
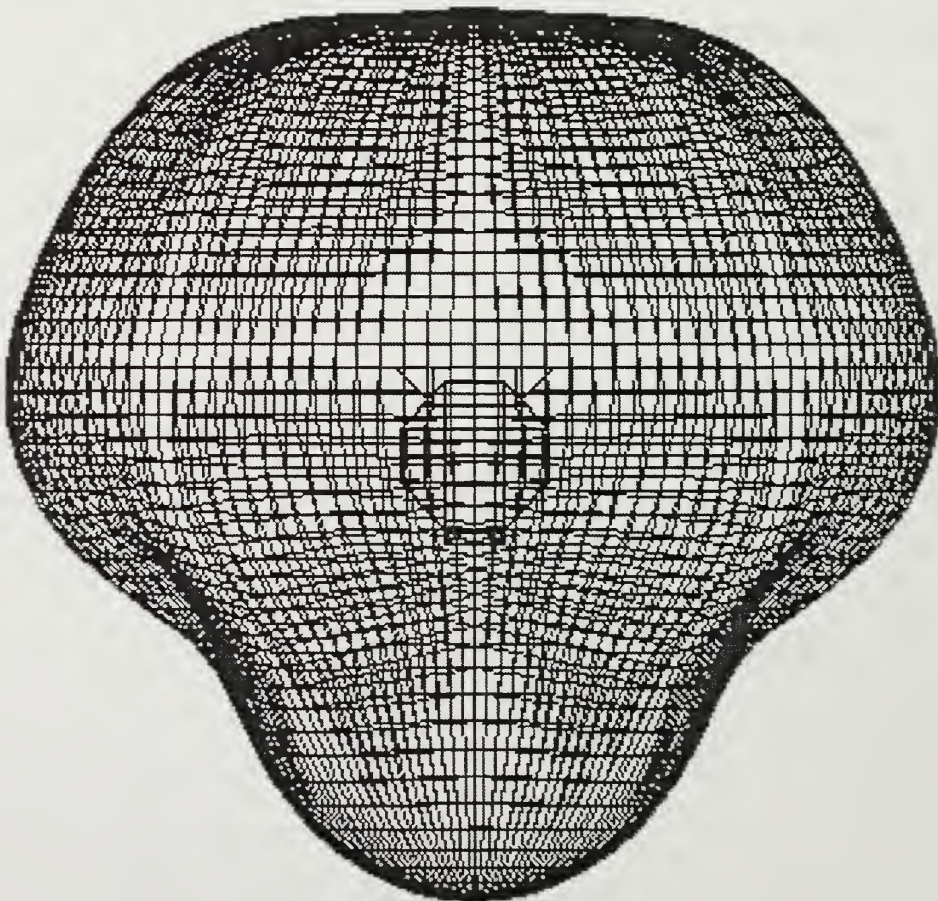
Figure 12 Original Design NEC 3D Surface Radiation Pattern Plot

The primary concern of this thesis was to reproduce this pattern with the physical elements and network integrated onto PANSAT. It has already been shown in previous chapters that both the elements and the feed network performed within their individual specifications. The next task was to set up valid tests and models which would be compared with each other. If, in the final analysis, these correlations were accurate, then the free-space NEC output for PANSAT could be utilized for both future modeling and tracking data.

The field testing was completed successfully on a large field. A wooden support for PANSAT was constructed so that the center of the scale model was approximately 171 cm from the ground. A picture of this setup is shown in Figure 13.
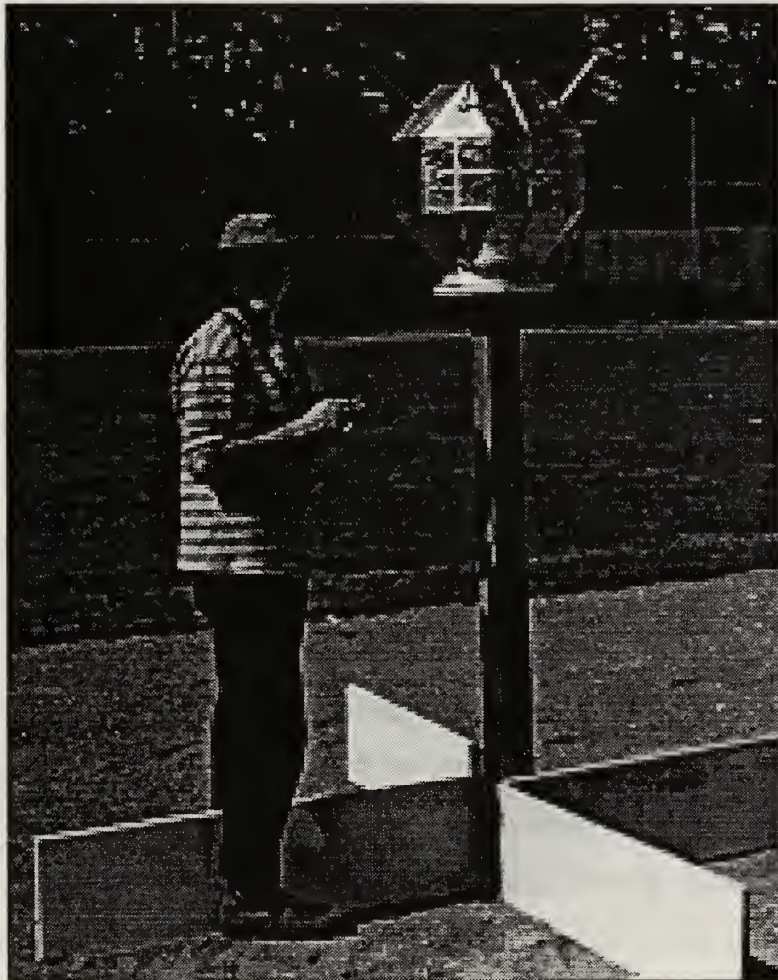
Figure 13 Test Setup

17

The base of the top support post has a printed circular angle guide that was used as a reference when rotating the model. Divisions were at 22.5° increments. The self contained power source of the model was a pack of six lead-acid batteries, 2 V each, providing a total of 5 amp-hours for the test and was attached to the center of the model with an aluminum bracket, providing center of mass stability. A Vectron oscillator and adapter circuit was then attached between the batteries and the feed network. The frequency for the oscillator was 437.25 MHz and its power output was measured at 12 dBm. This arrangement allowed for a completely self contained model that would not interfere with the radiation pattern generated by the antennas and the outer shell of the spacecraft.

The receiving antenna, tuned to this frequency, was placed ten meters away from the satellite. This distance satisfied the need to be at least ten wavelengths (7 m) away to measure the far-field pattern. For this field test, four variables were used to generate the data required to verify the radiation pattern. The first two are the angular rotations of the scale model. The angle θ_{rot} represents the rotation of the satellite from the +Z axis (straight up relative to the ground) which was varied from $0°$ to $135°$. The angle ϕ_{rot} (the direction in the x-y plane) was varied in 22.5° increments for most data, and $\pm 10°$ for fine tuning. These measurements had to be converted to the satellite-body coordinate system for analysis ($\phi_{sat} = 360° - \phi_{rot}$).

The last two variables were the polarization and the height of the receiving antenna. Since the pattern generated by the satellite has both vertical and horizontal components, they needed to be observed separately. This was accomplished by rotating the receiving antenna axis 90°. The height of the receiver was also adjusted so that the measurements were observed at three levels; the same height of the satellite, as well as $\pm \lambda/2$ (206 and 160 cm). This variation would account for the fact that the received signal was a combination of both the main lobe and the reflected energy from the flat, dirt surface of the field. It would also account for any possible nulls or maxima in the radiation pattern that might be missed with measurements at just one height. The complete description is shown in Figure 14 and Figure 15 on page 19.
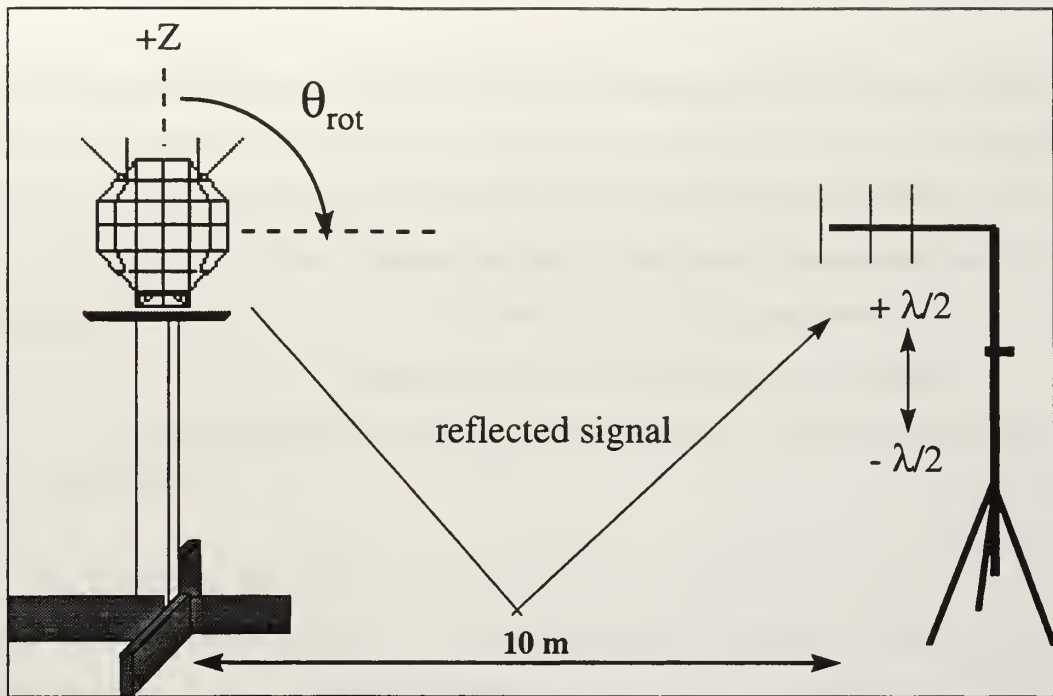
Figure 14 Field Test Side View
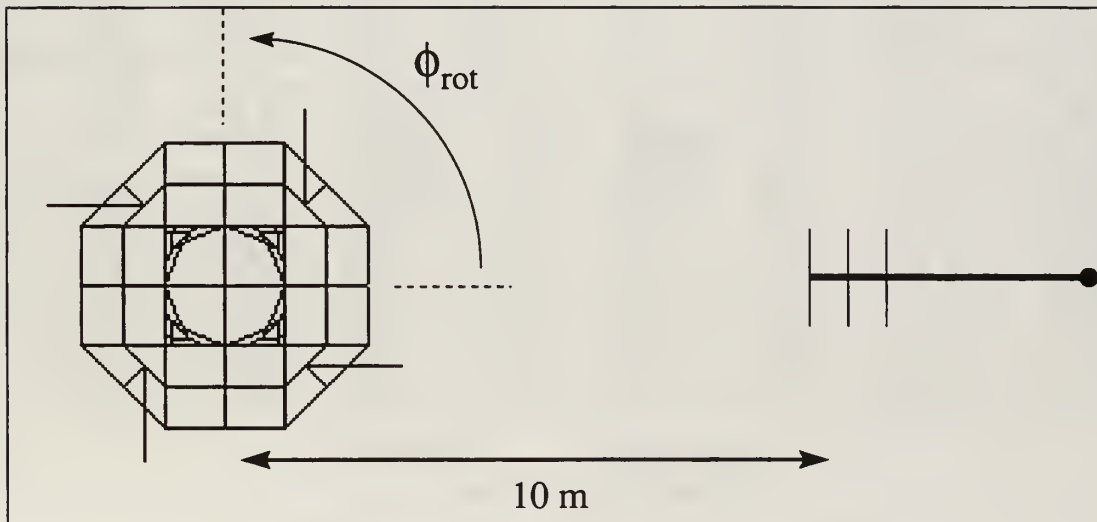
Figure 15 Field Test Top View

19

Therefore, the experimental data was comprised of the values of the received gain observed at:

1. Three different heights: level, $+\lambda/2$, $-\lambda/2$.
2. Two polarizations: Vertical and Horizontal.
3. Four variations of θ_{sat}: $0°$, $45°$, $90°$, $135°$.
4. Rotation of ϕ_{sat} through $360°$ in $22.5°$ intervals.

This data was collected and tabulated into spreadsheets (Appendix E) as illustrated below.

THETA =45

| | | OUTPUT (dB) | | | | | |
| | | 150 cm | | 171 cm | | 206 cm | |
PHI (deg)	PHI (rad)	VERT	HORIZ	VERT	HORIZ	VERT	HORIZ
0	0.00	-4.67	-5.50	-5.33	-7.83	-7.00	-6.17
22.5	0.39	-11.33	-2.00	-9.67	-6.50	-9.50	-4.67
45	0.79	-8.17	-1.17	-11.33	-5.33	-12.33	-4.83
67.5	1.18	-5.33	-2.17	-8.33	-6.33	-9.50	-5.00
90	1.57	-4.33	-2.33	-7.00	-6.50	-10.67	-5.17
112.5	1.96	-5.83	-0.60	-8.00	-5.17	-11.00	-4.33
135	2.36	-13.00	-2.33	-11.00	-6.33	-13.67	-4.00
157.5	2.75	-10.67	-3.67	-10.00	-9.17	-9.50	-6.17
180	3.14	-4.83	-1.50	-5.50	-6.33	-4.67	-6.33
202.5	3.53	-2.50	-3.33	-3.67	-9.33	-3.17	-7.17
225	3.93	-1.67	-17.00	-2.83	-12.67	-3.17	-16.00
247.5	4.32	-1.33	-3.17	-2.50	-6.33	-3.50	-10.00
270	4.71	-1.17	-8.67	-3.50	-13.33	-4.33	-10.33
292.5	5.11	-1.00	-12.67	-3.00	-11.50	-3.83	-16.00
315	5.50	-0.67	-6.00	-2.33	-7.50	-3.33	-14.67
337.5	5.89	-1.17	-7.33	-2.67	-7.80	-3.67	-10.83

Table 3 Field Test Data

Preliminary evaluation of the observed gain values were very promising. These measured values seem to match the gain patterns of the NEC simulation very closely. Both the vertical and horizontal polarizations exhibited their maxima and minima at the expected rotation (ϕ_{sat}) angles. These results will be analyzed in greater depth in Part C of this chapter.

B.   MODELING

The purpose of the field test was to verify that the NEC model was producing a credible radiation pattern compared to the physical results of the scale model. To simulate the field test, the original NEC simulation was modified so that the satellite was placed over a ground plane at the equivalent height (171 cm) and excited at the same frequency as the field test model (437.25 MHz). The NEC model was also rotated through the same θ_{sat} as the field test (0°, 45°, 90°, 135°) The ground plane was characterized in NEC to simulate the dirt field by inserting values for the dielectric constant for the ground in the vicinity of the antenna (ε) and the conductivity in mhos/meter of the ground in the vicinity of the antenna (σ). These would help simulate a comparable condition for the gains due to addition of the reflected waves. Figure 16 shows this configuration in NEC.
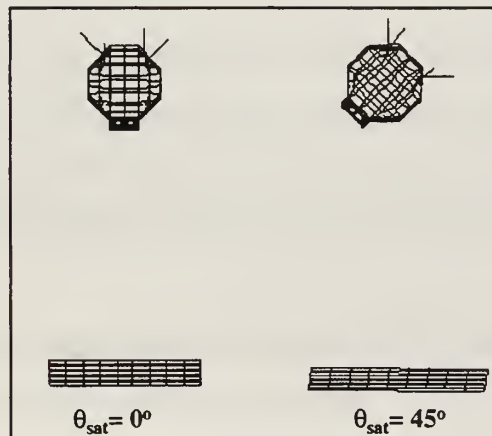
Figure 16 NEC Model of PANSAT over Ground Plane

This new model was then run on NEC and both the surface and gain patterns plotted for later comparison. The surface plot for a NEC field test model is shown below in Figure 17.
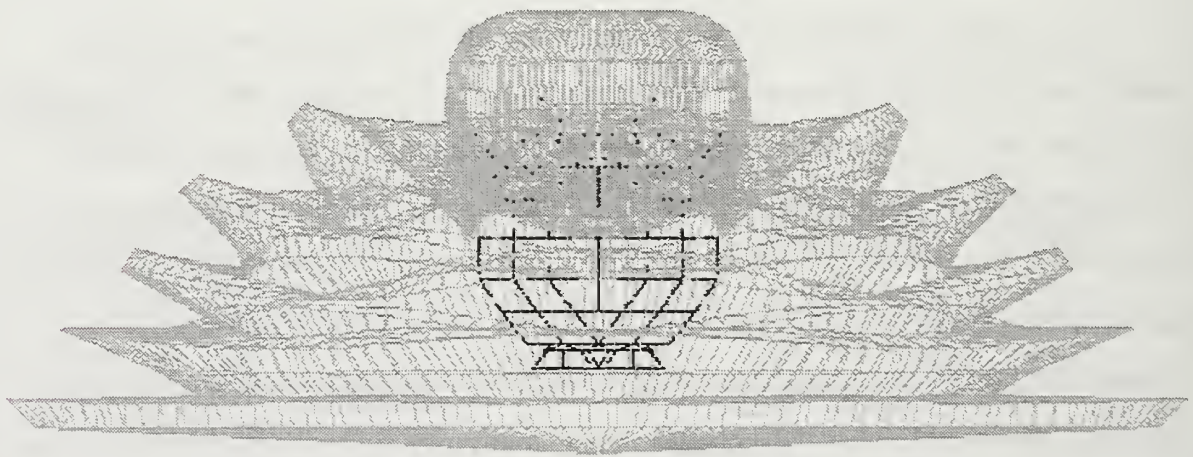
Figure 17 Field Test Surface Plot ($\phi_{sat} = 45^\circ$)

C.   COMPARISONS

The free-space radiation pattern for the original design was shown in Figure 12. The model for this final design with the new blade antennas was also generated by NEC to make a preliminary judgment whether or not the two were comparable. As can be seen, the two plots shown below in Figure 18, are very close in their general shape. This was the first confirmation that the new antennas would create the same general radiation pattern as the original theoretical design.

ORIGINAL DESIGN   **NEW ANTENNAS**
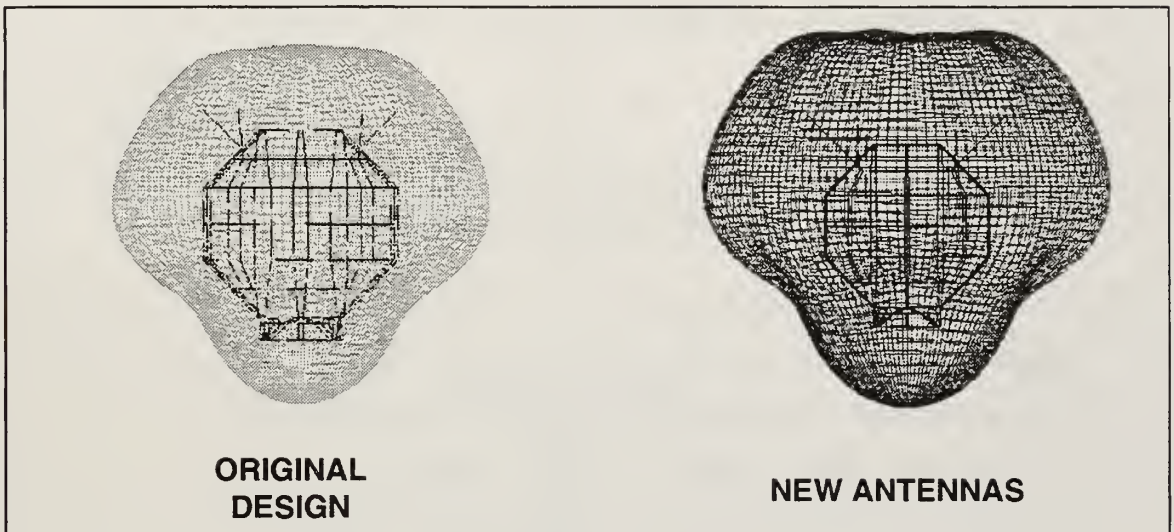
Figure 18 Surface Plots for Original and New Designs

The field test data was then tabulated and plotted so that a comparison could be made of their respective patterns. The Matlab function Polarhg.m (Appendix D) was utilized to plot all values of gain observed during the field test. This function was found on the Internet since the normal polar plotting routine could not handle negative numbers for radial distances.

An example of this comparison is shown Figure 19 and Figure 20 as the horizontal gains are plotted in both NEC and Matlab.

23
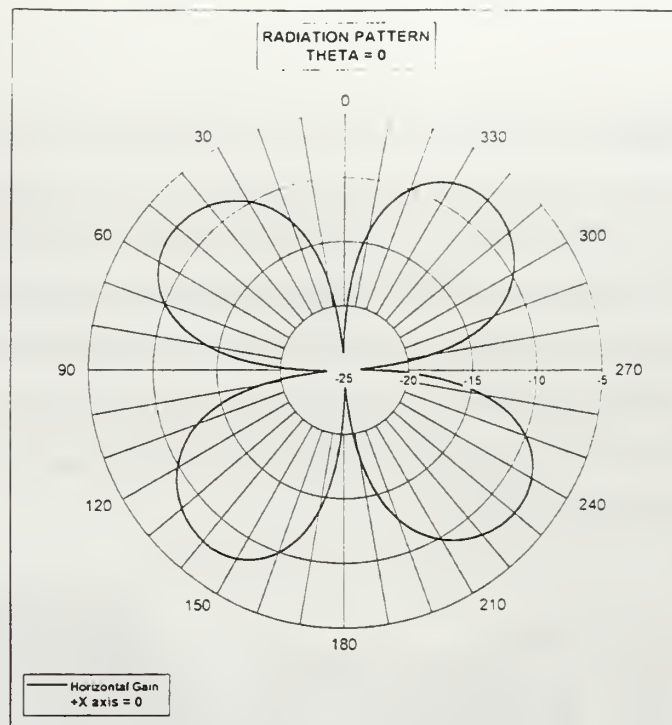
Figure 19 NEC Model of Field Test
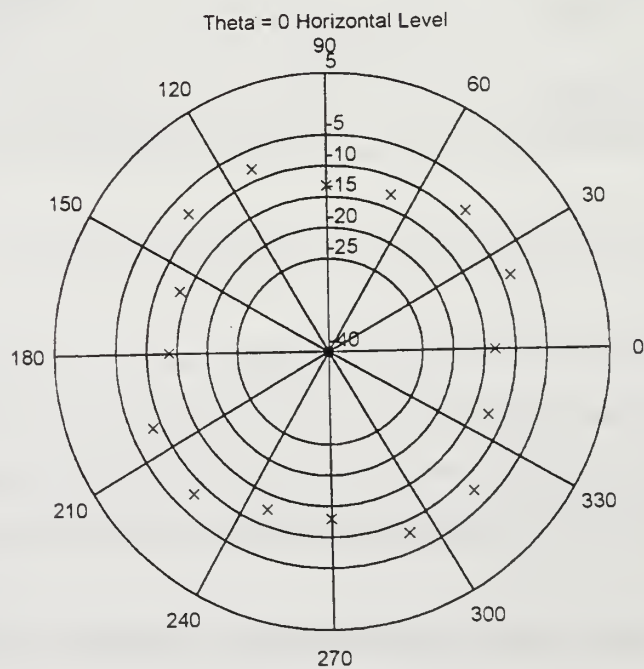
Figure 20 Matlab Data Plot (Horizontal Only)

This horizontal polarization plot (Figure 20) in Matlab demonstrates how the final test results compare with the NEC gain pattern. The shape of the field test pattern and the angles of the nulls and maxima match the NEC modeled output within tolerances to be considered a match. A plot of the three different measurement heights is shown in Figure 21 - 23 on page 24. These are also included in Appendix F. The differences in numerical and angular values for these plots were due to:

1. Their different input power values.
2. The physical characteristics of the field setup (ground characteristics, reflective surfaces).
3. Angular (field test) measuring accuracy.
4. Physical differences in the blade antenna configurations.

The primary function of these plots is to directly compare each aspect of the radiation pattern generated by NEC with the vertical, horizontal and total gain patterns. The secondary purpose is for satellite tracking by the ground station. These values and patterns as listed in Appendix G and will be used as a reference guide to compare PANSAT's relative attitude position as it tumbles. Although the solar panel output will be the primary source of attitude tracking, these gain values will be a reliable alternate source.

The physical testing in the field, together with the comparison of NEC modeling, successfully proved the validity of the NEC modeling and thus the final free-space radiation pattern. It is this final pattern and its values which will be utilized to help determine the spacecraft's attitude, assess link budget margins, and predict results of desired changes to PANSAT's antenna configuration.
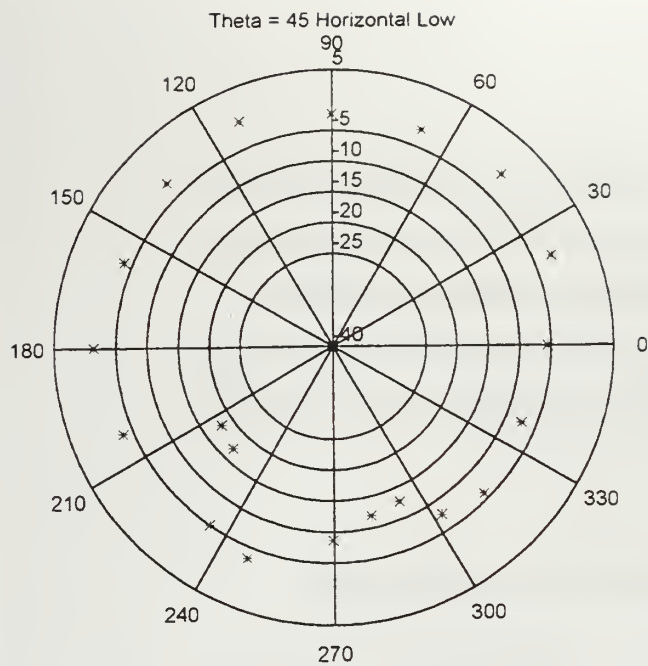
Figure 21 Field Test-Low
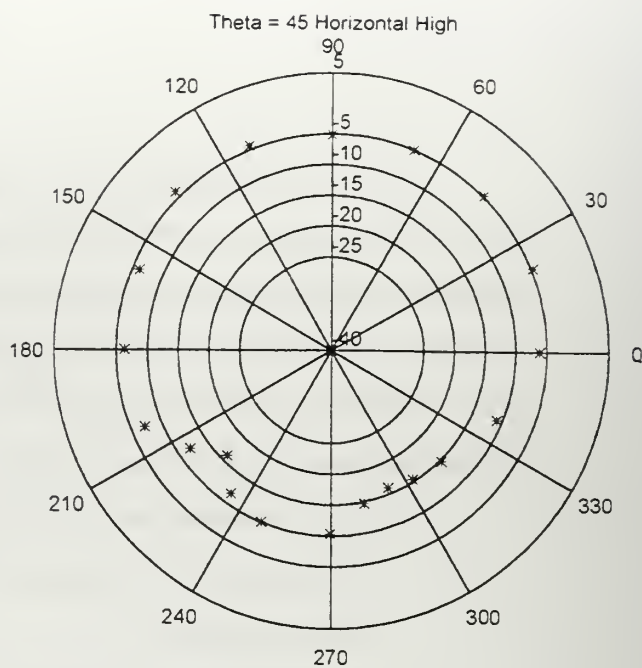
Figure 22 Field Test-High
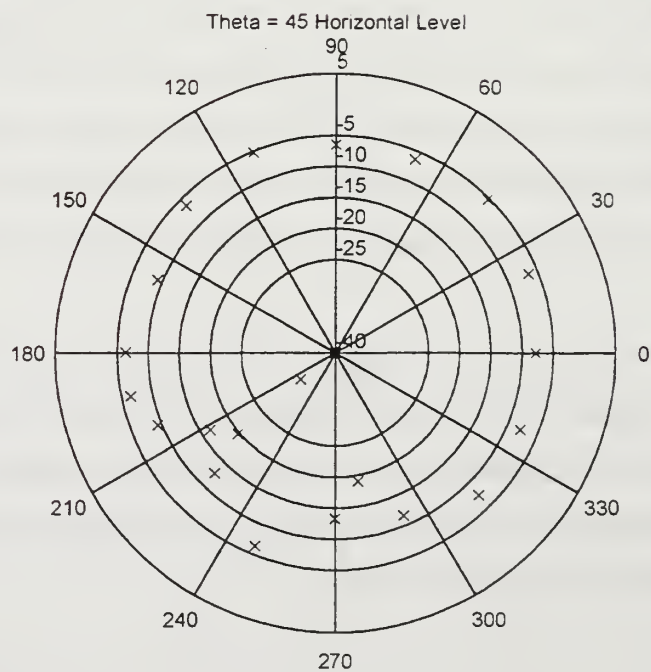
Figure 23 Field Test-Level ($\theta_{sat}=45^o$)

26

V. CONCLUSIONS AND RECOMMENDATIONS

A. DESIGN AND VALIDATION

The field tests and NEC models validated all three phases of the final antenna and matching network design. First, these comparisons proved that (1) the new, deployable blade antenna design was an applicable manifestation of the original, modeled antenna, (2) the simple feed network constructed of power and phase dividers (one 180° and two quad-hybrids) provided the symmetric radiation pattern and the impedance matching that was required, and (3) that these elements integrated onto the satellite and field tested proved that the NEC model could be utilized for later evaluation and tracking of the actual space flight of PANSAT.

B. LINK BUDGET AND DEPLOYMENT

The original comparison of the surface plots for the free-space models showed that they were very similar and validated the new design. The gain pattern for the new design shows that there is a minimum total gain of -8 dB at the top of the satellite where the antennas are attached. The maximum is 5 dB at the bottom of the LVI. Figure 24 shows the gain pattern for a ϕ_{sat} of 45°. This figure is also included in the Ground Station Reference Section in Appendix F.

The minimum output power gain generated by NEC for this final design (-8dB) eliminates the 6dB link margin originally calculated. This low gain value is only at the very top center of the satellite and increases significantly within 20° in each direction. The result of such a low gain will be signal fading or total loss as the spacecraft tumbles through this attitude.

It is estimated that the increased drag of the LVI will act as a "rudder" once the satellite is in orbit, and over time (the 2 year orbit) will stabilize PANSAT into an orbital configuration with the LVI in the flight vector direction as shown in Figure 25 on page 28.
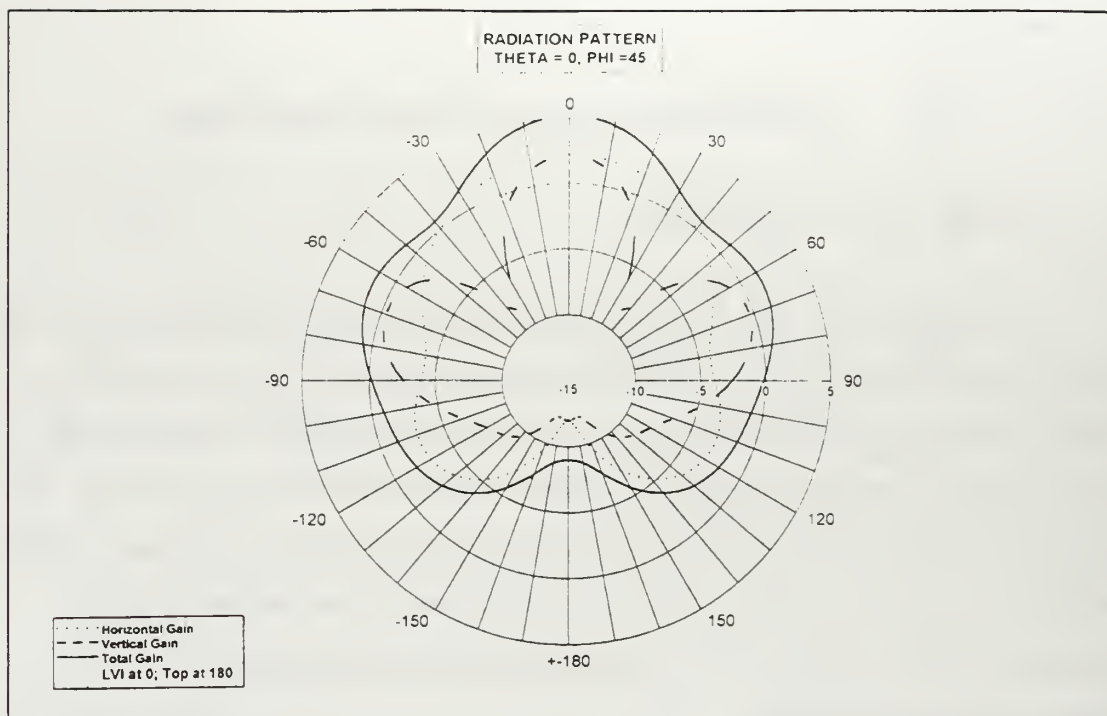
Figure 24 Gain Pattern for New Design
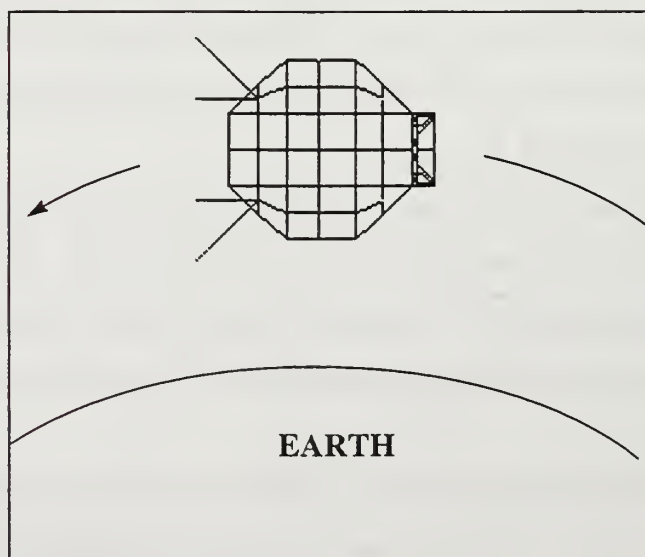
Figure 25 PANSAT's Predicted Attitude

If this attitude does develop as predicted, then the section of the pattern facing the earth station will be the $\pm\,90°$ ϕ_{sat} of the satellite (midsection). The gains at these angles range from -2 to +3 dB and will restore the 6 dB link margin. The deepest null other than the top of the spacecraft is +1 dB located approximately at $\theta_{sat} = 135°$ and $\phi_{sat} = 45°$ in all four symmetric quadrants and is also supportive of the link margin. The values for gain discussed have been total gains; the composition of the vertical and horizontal components.

The ground station will be able to track circular polarization, as well as these components. With this information, the operators of the station will be able to determine possible fade time as well as optimum receive antenna polarization. Of course, if the tumbling attitude and rate remains unpredictable, then the information provided in Appendix F and the power output from the solar cells can be used in conjunction only to approximate the present attitude and not predict impending fading and signal loss occurrences. The ejection attitude from the GAS canister as well as the LVI's increased drag greatly decreases the possibility that the +Z axis (top) will be directed at the earth station for any great length of time.

C.   CONCLUSIONS

The final antenna design and matching network as described in this thesis, satisfy the PANSAT specifications and will prove successful in its utilization. The new blade antennas match the original design in both impedance and radiation characteristics. Their flexibility also satisfies the pre-launch specification of fitting into the GAS canister. They are restrained until deployment by a filament attached to the end which is melted after PANSAT is ejected from the GAS canister. The final antenna impedances determined by NEC were approximately 100 Ω. This value is still within the manufacturer's guidelines for the matching network components to provide less than a 1.5: 1 SWR .

The matching network provides the necessary power division and phase shift between antennas to ensure a symmetric, free-space radiation pattern. Its small size required no major modifications to the PANSAT bus.

The final design free-space radiation pattern was validated by the comparison of the field test data and the patterns generated by NEC. This confirmation of the NEC models will allow the ground station to use the gain patterns and surface plots as an additional reference of PANSAT's attitude as it tumbles in orbit.

D.   RECOMMENDATIONS

The final space-flight PANSAT should be tested in a chamber to compare its final radiation pattern and power gains to those calculated in this thesis. If there are major differences in these values, the NEC model should be modified to match the space-flight PANSAT. This would ensure a stable reference for gain patterns and calculation of possible signal fading.

Additionally, the output power gain data from the free-space radiation pattern (Appendix F) should be integrated into the computer software of the ground station. This data is left for the software engineer as a matrix of 360° x 360° with 5° divisions. The comparison of power gains (or relative changes in gains) will allow for the determination of the attitude within at least one symmetric quadrant. Due to the symmetry of PANSAT's radiation pattern, only one quarter of this data is actually required for the software.

Finally, the matching network built for the field tests and validation used low power components (transmitter power only 12 dBm). Since the actual satellite will provide roughly 1-2 watts through the feed network, new quad-hybrids should be chosen to handle this increased power. The SWR of this feed network can be improved (reduced) if these new components have a higher power rating than the output of the rf system.

THETA = 0

		OUTPUT (dB)					
		150 cm		171 cm		206 cm	
PHI (deg)	PHI (rad)	VERT	HORIZ	VERT	HORIZ	VERT	HORIZ
0	0.00			-4.00	-13.33		
22.5	0.39			-5.50	-8.33		
45	0.79			-4.00	-8.33		
67.5	1.18			-2.00	-12.83		
90	1.57			-2.50	-13.17		
112.5	1.96			-4.33	-8.00		
135	2.36			-4.17	-8.00		
157.5	2.75			-3.33	-13.67		
180	3.14			-4.00	-13.67		
202.5	3.53			-5.83	-8.50		
225	3.93			-4.00	-8.00		
247.5	4.32			-2.17	-12.50		
270	4.71			-2.67	-13.00		
292.5	5.11			-4.50	-8.00		
315	5.50			-4.33	-7.67		
337.5	5.89			-3.00	-12.50		

THETA =45

<table>
<tr><td colspan="8" align="center">OUTPUT (dB)</td></tr>
<tr><td></td><td></td><td colspan="2" align="center">150 cm</td><td colspan="2" align="center">171 cm</td><td colspan="2" align="center">206 cm</td></tr>
<tr><td>PHI (deg)</td><td>PHI (rad)</td><td>VERT</td><td>HORIZ</td><td>VERT</td><td>HORIZ</td><td>VERT</td><td>HORIZ</td></tr>
<tr><td>0</td><td>0.00</td><td>-4.67</td><td>-5.50</td><td>-5.33</td><td>-7.83</td><td>-7.00</td><td>-6.17</td></tr>
<tr><td>22.5</td><td>0.39</td><td>-11.33</td><td>-2.00</td><td>-9.67</td><td>-6.50</td><td>-9.50</td><td>-4.67</td></tr>
<tr><td>45</td><td>0.79</td><td>-8.17</td><td>-1.17</td><td>-11.33</td><td>-5.33</td><td>-12.33</td><td>-4.83</td></tr>
<tr><td>67.5</td><td>1.18</td><td>-5.33</td><td>-2.17</td><td>-8.33</td><td>-6.33</td><td>-9.50</td><td>-5.00</td></tr>
<tr><td>90</td><td>1.57</td><td>-4.33</td><td>-2.33</td><td>-7.00</td><td>-6.50</td><td>-10.67</td><td>-5.17</td></tr>
<tr><td>112.5</td><td>1.96</td><td>-5.83</td><td>-0.60</td><td>-8.00</td><td>-5.17</td><td>-11.00</td><td>-4.33</td></tr>
<tr><td>135</td><td>2.36</td><td>-13.00</td><td>-2.33</td><td>-11.00</td><td>-6.33</td><td>-13.67</td><td>-4.00</td></tr>
<tr><td>157.5</td><td>2.75</td><td>-10.67</td><td>-3.67</td><td>-10.00</td><td>-9.17</td><td>-9.50</td><td>-6.17</td></tr>
<tr><td>180</td><td>3.14</td><td>-4.83</td><td>-1.50</td><td>-5.50</td><td>-6.33</td><td>-4.67</td><td>-6.33</td></tr>
<tr><td>202.5</td><td>3.53</td><td>-2.50</td><td>-3.33</td><td>-3.67</td><td>-9.33</td><td>-3.17</td><td>-7.17</td></tr>
<tr><td>225</td><td>3.93</td><td>-1.67</td><td>-17.00</td><td>-2.83</td><td>-12.67</td><td>-3.17</td><td>-16.00</td></tr>
<tr><td>247.5</td><td>4.32</td><td>-1.33</td><td>-3.17</td><td>-2.50</td><td>-6.33</td><td>-3.50</td><td>-10.00</td></tr>
<tr><td>270</td><td>4.71</td><td>-1.17</td><td>-8.67</td><td>-3.50</td><td>-13.33</td><td>-4.33</td><td>-10.33</td></tr>
<tr><td>292.5</td><td>5.11</td><td>-1.00</td><td>-12.67</td><td>-3.00</td><td>-11.50</td><td>-3.83</td><td>-16.00</td></tr>
<tr><td>315</td><td>5.50</td><td>-0.67</td><td>-6.00</td><td>-2.33</td><td>-7.50</td><td>-3.33</td><td>-14.67</td></tr>
<tr><td>337.5</td><td>5.89</td><td>-1.17</td><td>-7.33</td><td>-2.67</td><td>-7.80</td><td>-3.67</td><td>-10.83</td></tr>
<tr><td></td><td></td><td></td><td></td><td></td><td></td><td></td><td></td></tr>
<tr><td>192</td><td>3.35</td><td></td><td></td><td></td><td>-6.50</td><td></td><td></td></tr>
<tr><td>212</td><td>3.70</td><td></td><td></td><td></td><td>-16.50</td><td></td><td></td></tr>
<tr><td>217</td><td>3.79</td><td></td><td></td><td></td><td>-33.00</td><td></td><td></td></tr>
<tr><td>220</td><td>3.84</td><td></td><td></td><td></td><td>-19.67</td><td></td><td></td></tr>
<tr><td>280</td><td>4.89</td><td></td><td></td><td></td><td>-19.00</td><td></td><td></td></tr>
<tr><td></td><td></td><td></td><td></td><td></td><td></td><td></td><td></td></tr>
<tr><td>215</td><td>3.75</td><td></td><td>-18.00</td><td></td><td></td><td></td><td>-12.00</td></tr>
<tr><td>235</td><td>4.10</td><td></td><td>-5.00</td><td></td><td></td><td></td><td>-11.67</td></tr>
<tr><td>282.5</td><td>4.93</td><td></td><td>-12.00</td><td></td><td></td><td></td><td>-14.67</td></tr>
<tr><td>302.5</td><td>5.28</td><td></td><td>-7.67</td><td></td><td></td><td></td><td>-15.33</td></tr>
<tr><td></td><td></td><td></td><td></td><td></td><td></td><td></td><td></td></tr>
<tr><td>125</td><td>2.18</td><td>-11.00</td><td></td><td></td><td></td><td>-13.67</td><td></td></tr>
<tr><td>145</td><td>2.53</td><td>-14.17</td><td></td><td></td><td></td><td>-13.00</td><td></td></tr>
<tr><td>170</td><td>2.97</td><td></td><td></td><td></td><td></td><td>-6.00</td><td></td></tr>
<tr><td>190</td><td>3.32</td><td></td><td></td><td></td><td></td><td>-3.50</td><td></td></tr>
</table>

THETA = 90

<table>
<thead>
<tr><th rowspan="2">PHI (deg)</th><th rowspan="2">PHI (rad)</th><th colspan="6">OUTPUT (dB)</th></tr>
</thead>
</table>

PHI (deg)	PHI (rad)	150 cm VERT	150 cm HORIZ	171 cm VERT	171 cm HORIZ	206 cm VERT	206 cm HORIZ
0	0.00	-1.33	-2.50	-1.67	-5.67	-2.67	-6.17
22.5	0.39	-3.17	-4.00	-2.17	-9.17	-3.17	-6.67
45	0.79	-6.33	-3.33	-5.17	-6.50	-5.00	-10.27
67.5	1.18	-12.83	-1.83	-10.83	-5.00	-8.83	-12.67
90	1.57	-28.00	-0.50	-26.33	-4.00	-15.83	-9.67
112.5	1.96	-13.17	-1.33	-11.60	-1.83	-9.67	-8.67
135	2.36	-3.50	-2.83	-4.33	-4.50	-4.83	-8.67
157.5	2.75	0.17	-2.83	-2.00	-6.67	-2.17	-13.67
180	3.14	0.67	-1.50	-1.83	-1.83	-2.33	-6.00
202.5	3.53	-0.50	-1.83	-2.67	-5.50	-3.83	-9.00
225	3.93	-4.50	-5.67	-5.50	-12.50	-6.83	-11.17
247.5	4.32	-15.33	0.67	-10.00	-3.00	-13.67	-2.67
270	4.71	-13.33	-1.00	-19.80	-4.67	-25.00	-4.17
292.5	5.11	-6.83	-5.33	-9.50	-9.00	-9.83	-7.00
315	5.50	-2.67	-5.00	-5.50	-6.50	-5.83	-4.83
337.5	5.89	-1.17	-2.83	-5.50	-5.33	-3.67	-7.00
82	1.43			-14.70		-13.83	
100	1.75			-16.50		-15.87	
260	4.54			-16.70		-19.33	
282	4.92			-11.00		-15.67	
12.5	0.22				-8.00		
170	2.97				-3.00		
215	3.75				-15.67		
235	4.10				-5.00		
205	3.58				-10.00		
210	3.67		-4.50				
215	3.75		-7.13				
235	4.10		-2.50				
260	4.54		-3.50				
145	2.53						-11.17
147.5	2.57						-13.50
237	4.14						-4.00
57	0.99	-9.33					
77	1.34	-17.00					
100	1.75	-18.60					
237	4.14	-9.50					
257	4.49	-19.00					

THETA =135

PHI (deg)	PHI (rad)	OUTPUT (dB)					
		150 cm		171 cm		206 cm	
		VERT	HORIZ	VERT	HORIZ	VERT	HORIZ
0	0.00	-2.67	-3.67	-2.50	-7.33	-3.33	-15.67
22.5	0.39	-1.00	-8.67	-1.00	-15.00	-1.33	-11.00
45	0.79	-1.50	-14.60	-1.17	-18.50	-1.67	-7.83
67.5	1.18	-4.50	-11.00	-3.83	-14.00	-3.83	-12.67
90	1.57	-5.67	-4.00	-5.50	-7.00	-5.83	-18.00
112.5	1.96	-3.50	-2.17	-3.83	-5.00	-4.17	-13.00
135	2.36	-1.33	-9.00	-3.67	-12.00	-3.00	-22.00
157.5	2.75	-1.83	-3.67	-2.33	-5.33	-3.83	-9.33
180	3.14	-6.00	-2.00	-5.50	-3.83	-7.17	-5.83
202.5	3.53	-20.17	-3.33	-21.67	-5.17	-22.00	-6.33
225	3.93	-8.50	-0.17	-7.50	-2.50	-6.50	-8.17
247.5	4.32	-3.50	0.67	-2.17	-2.00	-2.33	-6.33
270	4.71	-2.50	-0.33	-2.00	-3.50	-2.00	-7.17
292.5	5.11	-4.00	-1.50	-3.33	-5.00	-5.33	-10.67
315	5.50	-11.00	-0.17	-11.83	-2.67	-13.67	-7.67
337.5	5.89	-9.67	-0.33	-9.00	-3.00	-6.83	-9.00
192	3.35	-11.00		-9.50			
212	3.70	-14.50		-15.00			
235	4.10			-3.50			
305	5.32			-6.00			
325	5.67			-15.17			
350	6.11			-4.67			
35	0.61				-12.50		
100	1.75				-31.00		
280	4.89				-11.00		
12	0.21		-5.50				
55	0.96		-18.00				
80	1.40		-6.83				
125	2.18		-5.67				
350	6.11		-1.87				
80	1.40						-16.47
100	1.75						-13.67
85	1.48						-25.00
125	2.18						-16.50
145	2.53						-20.33
190	3.32					-10.33	
192	3.35					-15.00	
212	3.70					-11.17	
305	5.32	-6.50				-9.00	
325	5.67	-17.60				-14.50	

APPENDIX B. FINAL DESIGN NEC INPUT FILE

```
CM FILE IS CALLED FINAL.NEC FROM C DRIVE THIS WORKS
CM THIS IS THE COMPLETE CONFIGURATION FOR PANSAT WITH ANTENNAS
CM 45 DEG. FROM XY PANE TILTED.(TO THE -z DIRECTION)
CM ANTENNAS WERE TESTED ON GROUND PLANE THEN
CM MODELED INTO THIS PROGRAM
CM LENGTHS ARE 21 CM IN ADDITION TO REACTANCE
CE
GW1,2,.218,0.,-.108,.218,0.,-.024,.007,
GW2,2,.218,0.,-.024,.218,0.,.06,.007,
GW3,2,.218,0.,-.024,.218,-.09,-.024,.007,
GW4,2,.218,0.,-.024,.218,.09,-.024,.007,
GW5,2,.218,.09,.06,.218,0.,.06,.007,
GW6,2,.156,.092,.127,.156,0.,.127,.007,
GW7,2,.218,-.09,.06,.218,0.,.06,.007,
GW8,2,.156,0.,.127,.156,-.092,.127,.007,
GW9,2,.218,.09,.06,.156,.092,.127,.005,
GW10,2,.218,0.,.06,.156,0.,.127,.007,
GW11,2,.218,-.09,.06,.156,-.092,.127,.005,
GW12,2,.09,.09,.194,.156,.092,.127,.005,
GW13,2,.156,0.,.127,.09,0.,.194,.007,
GW14,2,.09,-.09,.194,.156,-.092,.127,.005,
GW15,2,.218,-.09,-.108,.218,0.,-.108,.007,
GW16,2,.156,-.092,-.175,.156,0.,-.175,.007,
GW17,2,.218,.09,-.108,.218,0.,-.108,.007,
GW18,2,.156,0.,-.175,.156,.092,-.175,.007,
GW19,2,.218,-.09,-.108,.156,-.092,-.175,.005,
GW20,2,.218,0.,-.108,.156,0.,-.175,.007,
GW21,2,.218,.09,-.108,.156,.092,-.175,.005,
GW22,2,.09,-.09,-.242,.156,-.092,-.175,.005,
GW23,2,.156,0.,-.175,.09,0.,-.242,.007,
GW24,2,.09,.09,-.242,.156,.092,-.175,.005,
GW25,2,.218,.09,-.108,.218,.09,-.024,.007,
GW26,2,.154,.154,-.108,.154,.154,-.024,.007,
GW27,2,.218,.09,.06,.218,.09,-.024,.007,
GW28,2,.154,.154,-.024,.154,.154,.06,.007,
GW29,2,.218,.09,-.108,.154,.154,-.108,.005,
GW30,2,.218,.09,-.024,.154,.154,-.024,.007,
GW31,2,.218,.09,.06,.154,.154,.06,.005,
GW32,2,.09,.218,-.108,.154,.154,-.108,.005,
GW33,2,.154,.154,-.024,.09,.218,-.024,.007,
GW34,2,.09,.218,.06,.154,.154,.06,.005,
GW35,2,.218,-.09,-.108,.218,-.09,-.024,.007,
GW36,2,.154,-.154,-.108,.154,-.154,-.024,.007,
GW37,2,.218,-.09,.06,.218,-.09,-.024,.007,
GW38,2,.154,-.154,-.024,.154,-.154,.06,.007,
GW39,2,.218,-.09,-.108,.154,-.154,-.108,.005,
GW40,2,.218,-.09,-.024,.154,-.154,-.024,.007,
GW41,2,.218,-.09,.06,.154,-.154,.06,.005,
GW42,2,.09,-.218,-.108,.154,-.154,-.108,.005,
GW43,2,.154,-.154,-.024,.09,-.218,-.024,.007,
GW44,2,.09,-.218,.06,.154,-.154,.06,.005,
GW45,2,-.09,.218,-.024,0.,.218,-.024,.007,
GW46,2,.09,.218,-.024,0.,.218,-.024,.007,
GW47,2,0.,.218,-.024,0.,.218,.06,.007,
GW48,2,.09,.218,.06,.09,.218,-.024,.007,
GW49,2,0.,.218,-.024,0.,.218,-.108,.007,
GW50,2,.09,.218,-.108,.09,.218,-.024,.007,
GW51,2,-.09,.218,-.108,0.,.218,-.108,.007,
GW52,2,-.092,.156,-.175,0.,.156,-.175,.007,
GW53,2,.09,.218,-.108,0.,.218,-.108,.007,
GW54,2,0.,.156,-.175,.092,.156,-.175,.007,
GW55,2,-.09,.218,-.108,-.092,.156,-.175,.005,
GW56,2,0.,.218,-.108,0.,.156,-.175,.007,
GW57,2,.09,.218,-.108,.092,.156,-.175,.005,
GW58,2,-.09,.09,-.242,-.092,.156,-.175,.005,
```

```
GW59,2,0.,.156,-.175,0.,.09,-.242,.007,
GW60,2,.09,.09,-.242,.092,.156,-.175,.005,
GW61,2,-.09,.218,.06,0.,.218,.06,.007,
GW62,2,-.092,.156,.127,0.,.156,.127,.007,
GW63,2,.09,.218,.06,0.,.218,.06,.007,
GW64,2,0.,.156,.127,.092,.156,.127,.007,
GW65,2,-.09,.218,.06,-.092,.156,.127,.005,
GW66,2,0.,.218,.06,0.,.156,.127,.007,
GW67,2,.09,.218,.06,.092,.156,.127,.005,
GW68,2,-.09,.09,.194,-.092,.156,.127,.005,
GW69,2,0.,.156,.127,0.,.09,.194,.007,
GW70,2,.09,.09,.194,.092,.156,.127,.005,
GW71,2,-.09,.218,-.108,-.09,.218,-.024,.007,
GW72,2,-.154,.154,-.108,-.154,.154,-.024,.007,
GW73,2,-.09,.218,.06,-.09,.218,-.024,.007,
GW74,2,-.154,.154,-.024,-.154,.154,.06,.007,
GW75,2,-.09,.218,-.108,-.154,.154,-.108,.005,
GW76,2,-.09,.218,-.024,-.154,.154,-.024,.007,
GW77,2,-.09,.218,.06,-.154,.154,.06,.005,
GW78,2,-.218,.09,-.108,-.154,.154,-.108,.005,
GW79,2,-.154,.154,-.024,-.218,.09,-.024,.007,
GW80,2,-.218,.09,.06,-.154,.154,.06,.005,
GW81,2,.09,.09,-.242,0.,.09,-.242,.007,
GW82,2, .09,0,-.242, 0,0,-.242, .007
GW83,2, -.09,.09,-.242, 0,.09,-.242, .007
GW84,2,0.,0.,-.242,-.09,0.,-.242,.007,
GW85,2,.09,.09,-.242,.09,0.,-.242,.007,
GW86,2,0.,.09,-.242,0.,0.,-.242,.007,
GW87,2,.09,-.09,-.242,.09,0.,-.242,.007,
GW88,2,0.,0.,-.242,0.,-.09,-.242,.007,
GW89,2,.09,-.09,-.242,0.,-.09,-.242,.007,
GW90,2,.092,-.156,-.175,0.,-.156,-.175,.007,
GW91,2,-.09,-.09,-.242,0.,-.09,-.242,.007,
GW92,2,0.,-.156,-.175,-.092,-.156,-.175,.007,
GW93,2,.09,-.09,-.242,.092,-.156,-.175,.005,
GW94,2,0.,-.09,-.242,0.,-.156,-.175,.007,
GW95,2,-.09,-.09,-.242,-.092,-.156,-.175,.005,
GW96,2,.09,-.218,-.108,.092,-.156,-.175,.005,
GW97,2,0.,-.156,-.175,0.,-.218,-.108,.007,
GW98,2,-.09,-.218,-.108,-.092,-.156,-.175,.005,
GW99,2,-.09,-.09,-.242,-.09,0.,-.242,.007,
GW100,2,-.156,-.092,-.175,-.156,0.,-.175,.007,
GW101,2,-.09,.09,-.242,-.09,0.,-.242,.007,
GW102,2,-.156,0.,-.175,-.156,.092,-.175,.007,
GW103,2,-.09,-.09,-.242,-.156,-.092,-.175,.005,
GW104,2,-.09,0.,-.242,-.156,0.,-.175,.007,
GW105,2,-.09,.09,-.242,-.156,.092,-.175,.005,
GW106,2,-.218,-.09,-.108,-.156,-.092,-.175,.005,
GW107,2,-.156,0.,-.175,-.218,0.,-.108,.007,
GW108,2,-.218,.09,-.108,-.156,.092,-.175,.005,
GW109,2,.09,.09,.194,0.,.09,.194,.006,
GW110,2,-.09,.09,.194,0.,.09,.194,.006,
GW111,2,.09,-.09,.194,.09,0.,.194,.006,
GW112,2,.09,.09,.194,.09,0.,.194,.006,
GW113,2,.09,-.09,.194,.092,-.156,.127,.005,
GW114,2,0.,-.09,.194,0.,-.156,.127,.007,
GW115,2,-.09,-.09,.194,-.092,-.156,.127,.005,
GW116,2,.09,-.218,.06,.092,-.156,.127,.005,
GW117,2,0.,-.156,.127,0.,-.218,.06,.007,
GW118,2,-.09,-.218,.06,-.092,-.156,.127,.005,
GW119,2,.09,-.09,.194,0.,-.09,.194,.006,
GW120,2,.092,-.156,.127,0.,-.156,.127,.007,
GW121,2,-.09,-.09,.194,0.,-.09,.194,.006,
GW122,2,0.,-.156,.127,-.092,-.156,.127,.007,
GW123,2,.09,-.218,-.108,.09,-.218,-.024,.007,
GW124,2,0.,-.218,-.108,0.,-.218,-.024,.007,
GW125,2,.09,-.218,.06,.09,-.218,-.024,.007,
GW126,2,0.,-.218,.06,0.,-.218,-.024,.007,
```

```
GW127,2,.09,-.218,-.108,0.,-.218,-.108,.007,
GW128,2,.09,-.218,-.024,0.,-.218,-.024,.007,
GW129,2,.09,-.218,.06,0.,-.218,.06,.007,
GW130,2,-.09,-.218,-.108,0.,-.218,-.108,.007,
GW131,2,0.,-.218,-.024,-.09,-.218,-.024,.007,
GW132,2,-.09,-.218,.06,0.,-.218,.06,.007,
GW133,2,-.09,-.218,.06,-.154,-.154,.06,.005,
GW134,2,-.09,-.218,-.024,-.154,-.154,-.024,.007,
GW135,2,-.09,-.218,-.108,-.154,-.154,-.108,.005,
GW136,2,-.218,-.09,.06,-.154,-.154,.06,.005,
GW137,2,-.154,-.154,-.024,-.218,-.09,-.024,.007,
GW138,2,-.218,-.09,-.108,-.154,-.154,-.108,.005,
GW139,2,-.09,-.218,.06,-.09,-.218,-.024,.007,
GW140,2,-.154,-.154,.06,-.154,-.154,-.024,.007,
GW141,2,-.09,-.218,-.108,-.09,-.218,-.024,.007,
GW142,2,-.154,-.154,-.024,-.154,-.154,-.108,.007,
GW143,2,-.09,-.09,.194,-.09,0.,.194,.006,
GW144,2,-.156,-.092,.127,-.156,0.,.127,.007,
GW145,2,-.09,.09,.194,-.09,0.,.194,.006,
GW146,2,-.156,0.,.127,-.156,.092,.127,.007,
GW147,2,-.09,-.09,.194,-.156,-.092,.127,.005,
GW148,2,-.09,0.,.194,-.156,0.,.127,.007,
GW149,2,-.09,.09,.194,-.156,.092,.127,.005,
GW150,2,-.218,-.09,.06,-.156,-.092,.127,.007,
GW151,2,-.156,0.,.127,-.218,0.,.06,.005
GW152,2,-.218,.09,.06,-.156,.092,.127,.005,
GW153,2,-.218,-.09,.06,-.218,0.,.06,.007,
GW154,2,-.218,-.09,-.024,-.218,0.,-.024,.007,
GW155,2,-.218,-.09,-.108,-.218,0.,-.108,.007,
GW156,2,-.218,.09,.06,-.218,0.,.06,.007,
GW157,2,-.218,.09,-.024,-.218,0.,-.024,.007,
GW158,2,-.218,.09,-.108,-.218,0.,-.108,.007,
GW159,2,-.218,-.09,.06,-.218,-.09,-.024,.007,
GW160,2,-.218,0.,.06,-.218,0.,-.024,.007,
GW161,2,-.218,.09,.06,-.218,.09,-.024,.007,
GW162,2,-.218,-.09,-.108,-.218,-.09,-.024,.007,
GW163,2,-.218,0.,-.108,-.218,0.,-.024,.007,
GW164,2,-.218,.09,-.108,-.218,.09,-.024,.007,
GW165,1,.092,-.156,.127,.124,-.124,.127,.003,
GW166,1,.156,-.092,.127,.124,-.124,.127,.003,
GW167,2,.154,-.154,.06,.124,-.124,.127,.006,
GW168,1,.156,.092,.127,.124,.124,.127,.003,
GW169,2,.154,.154,.06,.124,.124,.127,.006,
GW170,1,.092,.156,.127,.124,.124,.127,.003,
GW171,1,-.092,.156,.127,-.124,.124,.127,.003,
GW172,1,-.156,.092,.127,-.124,.124,.127,.003,
GW173,2,-.154,.154,.06,-.124,.124,.127,.006,
GW174,1,-.156,-.092,.127,-.124,-.124,.127,.003,
GW175,2,-.154,-.154,.06,-.124,-.124,.127,.006,
GW176,1,-.092,-.156,.127,-.124,-.124,.127,.003,
GW177,1,.092,-.156,-.175,.124,-.124,-.175,.003,
GW178,2,.154,-.154,-.108,.124,-.124,-.175,.006,
GW179,1,.156,-.092,-.175,.124,-.124,-.175,.003,
GW180,1,-.156,.092,-.175,-.124,.124,-.175,.003,
GW181,2,-.154,.154,-.108,-.124,.124,-.175,.006,
GW182,1,-.092,.156,-.175,-.124,.124,-.175,.003,
GW183,1,.092,.156,-.175,.124,.124,-.175,.003,
GW184,2,.154,.154,-.108,.124,.124,-.175,.006,
GW185,1,.156,.092,-.175,.124,.124,-.175,.003,
GW186,1,-.156,-.092,-.175,-.124,-.124,-.175,.003,
GW187,2,-.154,-.154,-.108,-.124,-.124,-.175,.006,
GW188,1,-.092,-.156,-.175,-.124,-.124,-.175,.003,
GW189,5, .124,-.124,-.175, .124,-.2725,-.3235, .0045,
GW190,5, .124,.124,-.175, .2725,.124,-.3235, .0045,
GW191,5, -.124,.124,-.175, -.124,.2725,-.3235, .0045,
GW192,5, -.124,-.124,-.175, -.2725,-.124,-.3235, .0045,
GW193,1,-.078,.09,.2448,-.038,.09,.208,.0016,
GW194,1,-.038,.09,.208,0.,.09,.194,.0035,
```

```
GW195,1,0.,.09,.194,.038,.09,.208,.0035,
GW196,1,.038,.09,.208,.078,.09,.2448,.0016,
GW197,1,-.09,.078,.2448,-.09,.038,.208,.0016,
GW198,1,-.09,.038,.208,-.09,0.,.194,.0035,
GW199,1,-.09,0.,.194,-.09,-.038,.208,.0035,
GW200,1,-.09,-.038,.208,-.09,-.078,.2448,.0016,
GW201,1,-.078,-.09,.2448,-.038,-.09,.208,.0016,
GW202,1,-.038,-.09,.208,0.,-.09,.194,.0035,
GW203,1,0.,-.09,.194,.038,-.09,.208,.0035,
GW204,1,.038,-.09,.208,.078,-.09,.2448,.0016,
GW205,1,.09,-.078,.2448,.09,-.038,.208,.0016,
GW206,1,.09,-.038,.208,.09,0.,.194,.0035,
GW207,1,.09,0.,.194,.09,.038,.208,.0035,
GW208,1,.09,.038,.208,.09,.078,.2448,.0016,
GW209,1,-.038,.09,.208,0.,.09,.208,.0021,
GW210,1,0.,.09,.208,.038,.09,.208,.0021,
GW211,1,-.078,.09,.2448,-.038,.09,.2448,.003,
GW212,1,-.038,.09,.2448,0.,.09,.2448,.003,
GW213,1,0.,.09,.2448,.038,.09,.2448,.003,
GW214,1,.038,.09,.2448,.078,.09,.2448,.003,
GW215,1,0.,.09,.2448,0.,.09,.208,.003,
GW216,1,-.09,-.078,.2448,-.09,-.038,.2448,.003,
GW217,1,-.09,-.038,.2448,-.09,0.,.2448,.003,
GW218,1,-.09,0.,.2448,-.09,.038,.2448,.003,
GW219,1,-.09,.038,.2448,-.09,.078,.2448,.003,
GW220,1,-.09,-.038,.208,-.09,0.,.208,.0021,
GW221,1,-.09,0.,.208,-.09,.038,.208,.0021,
GW222,1,-.09,0.,.2448,-.09,0.,.208,.003,
GW223,1,.078,-.09,.2448,.038,-.09,.2448,.003,
GW224,1,.038,-.09,.2448,0.,-.09,.2448,.003,
GW225,1,0.,-.09,.2448,-.038,-.09,.2448,.003,
GW226,1,-.038,-.09,.2448,-.078,-.09,.2448,.003,
GW227,1,0.,-.09,.2448,0.,-.09,.208,.003,
GW228,1,.038,-.09,.208,0.,-.09,.208,.0021,
GW229,1,0.,-.09,.208,-.038,-.09,.208,.0021,
GW230,1,.09,.078,.2448,.09,.038,.2448,.003,
GW231,1,.09,.038,.2448,.09,0.,.2448,.003,
GW232,1,.09,0.,.2448,.09,-.038,.2448,.003,
GW233,1,.09,-.038,.2448,.09,-.078,.2448,.003,
GW234,1,.09,0.,.2448,.09,0.,.208,.003,
GW235,1,.09,.038,.208,.09,0.,.208,.0021,
GW236,1,.09,0.,.208,.09,-.038,.208,.0021,
GW237,1,0.,.09,.194,-.0517,.0735,.194,.0021,
GW238,1,-.0517,.0735,.194,-.0636,.0636,.194,.0021,
GW239,1,-.0636,.0636,.194,-.0735,.0517,.194,.0021,
GW240,1,-.0735,.0517,.194,-.09,0.,.194,.0021,
GW241,1,-.09,0.,.194,-.0735,-.0517,.194,.0021,
GW242,1,-.0735,-.0517,.194,-.0636,-.0636,.194,.0021,
GW243,1,-.0636,-.0636,.194,-.0517,-.0735,.194,.0021,
GW244,1,-.0517,-.0735,.194,0.,-.09,.194,.0021,
GW245,1,0.,-.09,.194,.0517,-.0735,.194,.0021,
GW246,1,.0517,-.0735,.194,.0636,-.0636,.194,.0021,
GW247,1,.0636,-.0636,.194,.0735,-.0517,.194,.0021,
GW248,1,.0735,-.0517,.194,.09,0.,.194,.0021,
GW249,1,.09,0.,.194,.0735,.0517,.194,.0021,
GW250,1,.0735,.0517,.194,.0636,.0636,.194,.0021,
GW251,1,.0636,.0636,.194,.0517,.0735,.194,.0021,
GW252,1,.0517,.0735,.194,0.,.09,.194,.0021,
GW253,1,-.078,.09,.2448,-.0842,.0842,.2448,.0021,
GW254,1,-.0842,.0842,.2448,-.09,.078,.2448,.0021,
GW255,1,-.09,-.078,.2448,-.0842,-.0842,.2448,.0021,
GW256,1,-.0842,-.0842,.2448,-.078,-.09,.2448,.0021,
GW257,1,.078,-.09,.2448,.0842,-.0842,.2448,.0021,
GW258,1,.0842,-.0842,.2448,.09,-.078,.2448,.0021,
GW259,1,.09,.078,.2448,.0842,.0842,.2448,.0021,
GW260,1,.0842,.0842,.2448,.078,.09,.2448,.0021,
GW261,1,-.038,.09,.208,-.0545,.081,.208,.0021,
GW262,1,-.0545,.081,.208,-.069,.069,.208,.0021,
```

```
GW263,1,-.069,.069,.208,-.081,.0545,.208,.0021,
GW264,1,-.081,.0545,.208,-.09,.038,.208,.0021,
GW265,1,-.09,-.038,.208,-.081,-.0545,.208,.0021,
GW266,1,-.081,-.0545,.208,-.069,-.069,.208,.0021,
GW267,1,-.069,-.069,.208,-.0545,-.081,.208,.0021,
GW268,1,-.0545,-.081,.208,-.038,-.09,.208,.0021,
GW269,1,.038,-.09,.208,.0545,-.081,.208,.0021,
GW270,1,.0545,-.081,.208,.069,-.069,.208,.0021,
GW271,1,.069,-.069,.208,.081,-.0545,.208,.0021,
GW272,1,.081,-.0545,.208,.09,-.038,.208,.0021,
GW273,1,.09,.038,.208,.081,.0545,.208,.0021,
GW274,1,.081,.0545,.208,.069,.069,.208,.0021,
GW275,1,.069,.069,.208,.0545,.081,.208,.0021,
GW276,1,.0545,.081,.208,.038,.09,.208,.0021,
GW277,1,-.0545,.081,.208,-.0636,.0636,.194,.0021,
GW278,1,-.081,.0545,.208,-.0636,.0636,.194,.0021,
GW279,1,-.081,-.0545,.208,-.0636,-.0636,.194,.0021,
GW280,1,-.0545,-.081,.208,-.0636,-.0636,.194,.0021,
GW281,1,.0545,-.081,.208,.0636,-.0636,.194,.0021,
GW282,1,.081,-.0545,.208,.0636,-.0636,.194,.0021,
GW283,1,.081,.0545,.208,.0636,.0636,.194,.0021,
GW284,1,.0545,.081,.208,.0636,.0636,.194,.0021,
GW285,1,-.0842,.0842,.2448,-.0545,.081,.208,.0021,
GW286,1,-.0842,.0842,.2448,-.081,.0545,.208,.0021,
GW287,1,-.0842,-.0842,.2448,-.081,-.0545,.208,.0021,
GW288,1,-.0842,-.0842,.2448,-.0545,-.081,.208,.0021,
GW289,1,.0842,-.0842,.2448,.0545,-.081,.208,.0021,
GW290,1,.0842,-.0842,.2448,.081,-.0545,.208,.0021,
GW291,1,.0842,.0842,.2448,.081,.0545,.208,.0021,
GW292,1,.0842,.0842,.2448,.0545,.081,.208,.0021,
GW293,2,0.,-.09,.2448,0.,0.,.2448,.008,
GW294,2,-.09,0.,.2448,0.,0.,.2448,.008,
GW 295,2, 0.,-.09,.2448, 0.,0.,.2448, .008
GW 296,2, .09,0.,.2448, 0.,0.,.2448, .008
GE 0
FR 0 1 0 0 436.5 0
LD 4 189 1 1 0 -57,
LD 4 190 1 1 0 -57,
LD 4 191 1 1 0 -57,
LD 4 192 1 1 0 -57,
EX 0 189 2 00 1.
EX 0 190 2 00 0. 1.
EX 0 191 2 00 -1.
EX 0 192 2 00 0. -1.
RP 0 121 1 1000 0 0 3 0
RP 0 121 1 1000 0 45 3 1
RP 0 121 1 1000 0 90 3 1
RP 0 1 121 1000 90 0 1 3
EN
```

APPENDIX C. FINAL DESIGN NEC OUTPUT FILE

**** Power Gains: Theta Pattern ****
Phi=90, Freq=436.5, File=FINAL.DAT

**** Power Gains: Theta Pattern ****
Phi=45, Freq=436.5, File=FINAL.DAT

Theta Degrees	Horizontal dB	Vertical dB	Total dB	Theta Degrees	Horizontal dB	Vertical dB	Total dB
0.00	2.16	2.16	5.17	0.00	2.17	2.16	5.17
3.00	2.14	2.10	5.13	3.00	2.15	2.09	5.13
6.00	2.07	1.91	5.00	6.00	2.11	1.87	5.00
9.00	1.96	1.59	4.79	9.00	2.04	1.51	4.79
12.00	1.81	1.14	4.49	12.00	1.95	0.98	4.50
15.00	1.60	0.54	4.12	15.00	1.83	0.29	4.14
18.00	1.36	-0.20	3.66	18.00	1.69	-0.58	3.71
21.00	1.06	-1.10	3.12	21.00	1.53	-1.66	3.23
24.00	0.72	-2.15	2.53	24.00	1.34	-2.96	2.71
27.00	0.32	-3.34	1.88	27.00	1.13	-4.48	2.19
30.00	-0.12	-4.61	1.20	30.00	0.91	-6.11	1.69
33.00	-0.62	-5.76	0.54	33.00	0.66	-7.58	1.27
36.00	-1.17	-6.51	-0.06	36.00	0.40	-8.28	0.95
39.00	-1.79	-6.55	-0.53	39.00	0.12	-7.84	0.76
42.00	-2.46	-5.89	-0.83	42.00	-0.18	-6.62	0.71
45.00	-3.19	-4.84	-0.93	45.00	-0.50	-5.22	0.76
48.00	-4.00	-3.70	-0.84	48.00	-0.84	-3.95	0.89
51.00	-4.88	-2.63	-0.60	51.00	-1.19	-2.88	1.05
54.00	-5.84	-1.68	-0.27	54.00	-1.56	-2.03	1.22
57.00	-6.90	-0.88	0.09	57.00	-1.94	-1.38	1.36
60.00	-8.06	-0.21	0.45	60.00	-2.32	-0.90	1.46
63.00	-9.35	0.32	0.77	63.00	-2.70	-0.58	1.50
66.00	-10.78	0.74	1.04	66.00	-3.06	-0.40	1.48
69.00	-12.38	1.05	1.25	69.00	-3.39	-0.34	1.40
72.00	-14.22	1.27	1.39	72.00	-3.68	-0.40	1.27
75.00	-16.32	1.39	1.46	75.00	-3.90	-0.56	1.09
78.00	-18.71	1.42	1.47	78.00	-4.05	-0.81	0.87
81.00	-21.21	1.38	1.41	81.00	-4.12	-1.15	0.62
84.00	-22.92	1.27	1.29	84.00	-4.11	-1.57	0.36
87.00	-22.60	1.10	1.11	87.00	-4.03	-2.04	0.09
90.00	-20.84	0.86	0.89	90.00	-3.90	-2.58	-0.18
93.00	-18.90	0.58	0.63	93.00	-3.73	-3.16	-0.43
96.00	-17.22	0.27	0.35	96.00	-3.55	-3.77	-0.65
99.00	-15.83	-0.07	0.05	99.00	-3.37	-4.40	-0.85
102.00	-14.70	-0.41	-0.25	102.00	-3.21	-5.03	-1.02
105.00	-13.78	-0.75	-0.54	105.00	-3.08	-5.65	-1.17

108.00	-13.03	-1.07	-0.80	108.00	-2.99	-6.23	-1.30
111.00	-12.42	-1.37	-1.04	111.00	-2.94	-6.75	-1.43
114.00	-11.93	-1.64	-1.25	114.00	-2.94	-7.20	-1.56
117.00	-11.54	-1.89	-1.44	117.00	-3.00	-7.57	-1.70
120.00	-11.24	-2.12	-1.62	120.00	-3.11	-7.88	-1.86
123.00	-11.02	-2.36	-1.81	123.00	-3.27	-8.13	-2.04
126.00	-10.87	-2.62	-2.01	126.00	-3.50	-8.34	-2.27
129.00	-10.78	-2.91	-2.25	129.00	-3.78	-8.54	-2.53
132.00	-10.74	-3.24	-2.53	132.00	-4.12	-8.75	-2.83
135.00	-10.74	-3.64	-2.87	135.00	-4.52	-8.99	-3.19
138.00	-10.78	-4.11	-3.26	138.00	-4.97	-9.28	-3.60
141.00	-10.85	-4.65	-3.71	141.00	-5.47	-9.61	-4.05
144.00	-10.94	-5.27	-4.23	144.00	-6.02	-9.99	-4.56
147.00	-11.05	-5.97	-4.79	147.00	-6.62	-10.42	-5.10
150.00	-11.17	-6.74	-5.40	150.00	-7.25	-10.85	-5.68
153.00	-11.29	-7.56	-6.03	153.00	-7.90	-11.28	-6.26
156.00	-11.42	-8.41	-6.65	156.00	-8.57	-11.66	-6.84
159.00	-11.54	-9.26	-7.24	159.00	-9.24	-11.95	-7.38
162.00	-11.66	-10.04	-7.77	162.00	-9.88	-12.14	-7.85
165.00	-11.76	-10.72	-8.20	165.00	-10.48	-12.22	-8.25
168.00	-11.85	-11.26	-8.53	168.00	-11.00	-12.22	-8.56
171.00	-11.92	-11.63	-8.77	171.00	-11.44	-12.16	-8.77
174.00	-11.98	-11.87	-8.91	174.00	-11.76	-12.09	-8.91
177.00	-12.01	-11.98	-8.99	177.00	-11.96	-12.03	-8.99
180.00	-12.02	-12.02	-9.01	180.00	-12.03	-12.01	-9.01
183.00	-12.01	-11.98	-8.98	183.00	-11.96	-12.03	-8.98
186.00	-11.97	-11.86	-8.91	186.00	-11.76	-12.08	-8.91
189.00	-11.92	-11.62	-8.76	189.00	-11.44	-12.15	-8.77
192.00	-11.85	-11.25	-8.53	192.00	-11.01	-12.20	-8.55
195.00	-11.76	-10.71	-8.19	195.00	-10.48	-12.20	-8.25
198.00	-11.65	-10.03	-7.76	198.00	-9.88	-12.12	-7.85
201.00	-11.54	-9.24	-7.23	201.00	-9.24	-11.94	-7.37
204.00	-11.42	-8.40	-6.64	204.00	-8.58	-11.65	-6.84
207.00	-11.29	-7.55	-6.02	207.00	-7.91	-11.28	-6.26
210.00	-11.17	-6.73	-5.39	210.00	-7.25	-10.86	-5.68
213.00	-11.05	-5.96	-4.79	213.00	-6.62	-10.43	-5.11
216.00	-10.94	-5.26	-4.22	216.00	-6.02	-10.01	-4.56
219.00	-10.85	-4.64	-3.71	219.00	-5.47	-9.63	-4.06
222.00	-10.78	-4.10	-3.26	222.00	-4.96	-9.30	-3.60
225.00	-10.75	-3.64	-2.87	225.00	-4.51	-9.02	-3.19
228.00	-10.74	-3.24	-2.53	228.00	-4.12	-8.77	-2.84
231.00	-10.79	-2.91	-2.25	231.00	-3.78	-8.56	-2.53

234.00	-10.88	-2.62	-2.02	234.00	-3.49	-8.35	-2.27
237.00	-11.03	-2.37	-1.81	237.00	-3.27	-8.14	-2.05
240.00	-11.25	-2.13	-1.63	240.00	-3.10	-7.89	-1.86
243.00	-11.55	-1.89	-1.45	243.00	-2.99	-7.57	-1.70
246.00	-11.94	-1.64	-1.26	246.00	-2.94	-7.19	-1.56
249.00	-12.43	-1.37	-1.04	249.00	-2.94	-6.74	-1.43
252.00	-13.04	-1.07	-0.81	252.00	-2.99	-6.21	-1.30
255.00	-13.79	-0.75	-0.54	255.00	-3.08	-5.63	-1.16
258.00	-14.72	-0.41	-0.25	258.00	-3.21	-5.02	-1.01
261.00	-15.85	-0.07	0.05	261.00	-3.37	-4.38	-0.84
264.00	-17.24	0.27	0.35	264.00	-3.55	-3.75	-0.64
267.00	-18.92	0.59	0.64	267.00	-3.73	-3.14	-0.42
270.00	-20.87	0.87	0.90	270.00	-3.90	-2.56	-0.17
273.00	-22.65	1.10	1.12	273.00	-4.03	-2.03	0.10
276.00	-22.96	1.28	1.29	276.00	-4.10	-1.55	0.37
279.00	-21.22	1.39	1.41	279.00	-4.11	-1.14	0.63
282.00	-18.71	1.43	1.47	282.00	-4.05	-0.80	0.88
285.00	-16.31	1.39	1.47	285.00	-3.90	-0.55	1.10
288.00	-14.20	1.27	1.39	288.00	-3.67	-0.39	1.28
291.00	-12.37	1.06	1.25	291.00	-3.39	-0.34	1.41
294.00	-10.76	0.75	1.04	294.00	-3.05	-0.40	1.49
297.00	-9.33	0.33	0.78	297.00	-2.69	-0.58	1.50
300.00	-8.05	-0.21	0.45	300.00	-2.31	-0.90	1.46
303.00	-6.89	-0.87	0.10	303.00	-1.93	-1.38	1.36
306.00	-5.84	-1.67	-0.26	306.00	-1.55	-2.04	1.22
309.00	-4.87	-2.62	-0.59	309.00	-1.18	-2.89	1.05
312.00	-3.99	-3.70	-0.83	312.00	-0.83	-3.97	0.89
315.00	-3.19	-4.84	-0.92	315.00	-0.50	-5.25	0.76
318.00	-2.45	-5.89	-0.83	318.00	-0.18	-6.65	0.70
321.00	-1.78	-6.55	-0.53	321.00	0.12	-7.87	0.76
324.00	-1.17	-6.52	-0.06	324.00	0.40	-8.32	0.95
327.00	-0.62	-5.77	0.54	327.00	0.67	-7.61	1.27
330.00	-0.12	-4.62	1.20	330.00	0.91	-6.13	1.69
333.00	0.33	-3.35	1.88	333.00	1.14	-4.48	2.19
336.00	0.72	-2.16	2.53	336.00	1.34	-2.97	2.71
339.00	1.06	-1.10	3.12	339.00	1.53	-1.67	3.23
342.00	1.36	-0.20	3.66	342.00	1.69	-0.58	3.71
345.00	1.61	0.54	4.12	345.00	1.83	0.29	4.14
348.00	1.81	1.14	4.49	348.00	1.95	0.98	4.50
351.00	1.96	1.59	4.79	351.00	2.04	1.51	4.79
354.00	2.07	1.91	5.00	354.00	2.11	1.87	5.00
357.00	2.14	2.10	5.13	357.00	2.15	2.09	5.13

| 360.00 | 2.16 | 2.16 | 5.17 | | 360.00 | 2.17 | 2.16 | 5.17 |

**** Power Gains: Phi Pattern ****
Theta=45, Freq=436.5, File=FINAL.DAT

**** Power Gains: Phi Pattern ****
Theta=90, Freq=436.5, File=FINAL.DAT

Phi Degrees	Horizontal dB	Vertical dB	Total dB	Phi Degrees	Horizontal dB	Vertical dB	Total dB
0.00	-3.19	-4.84	-0.93	0.00	-20.87	0.87	0.89
3.00	-3.20	-5.12	-1.04	3.00	-16.61	0.82	0.90
6.00	-3.13	-5.41	-1.11	6.00	-13.41	0.72	0.88
9.00	-2.98	-5.70	-1.12	9.00	-11.04	0.57	0.86
12.00	-2.77	-5.99	-1.08	12.00	-9.23	0.36	0.81
15.00	-2.52	-6.25	-0.98	15.00	-7.81	0.11	0.76
18.00	-2.24	-6.46	-0.84	18.00	-6.69	-0.19	0.69
21.00	-1.94	-6.61	-0.67	21.00	-5.80	-0.53	0.60
24.00	-1.66	-6.68	-0.47	24.00	-5.10	-0.89	0.50
27.00	-1.39	-6.65	-0.26	27.00	-4.57	-1.27	0.40
30.00	-1.15	-6.54	-0.04	30.00	-4.18	-1.65	0.28
33.00	-0.94	-6.36	0.16	33.00	-3.91	-1.99	0.16
36.00	-0.77	-6.12	0.35	36.00	-3.76	-2.28	0.05
39.00	-0.64	-5.83	0.51	39.00	-3.71	-2.49	-0.05
42.00	-0.55	-5.53	0.65	42.00	-3.76	-2.59	-0.13
45.00	-0.50	-5.22	0.76	45.00	-3.90	-2.58	-0.18
48.00	-0.50	-4.93	0.84	48.00	-4.12	-2.46	-0.20
51.00	-0.54	-4.66	0.88	51.00	-4.42	-2.23	-0.18
54.00	-0.62	-4.43	0.89	54.00	-4.80	-1.94	-0.13
57.00	-0.75	-4.23	0.86	57.00	-5.27	-1.60	-0.05
60.00	-0.91	-4.07	0.80	60.00	-5.83	-1.24	0.05
63.00	-1.11	-3.96	0.71	63.00	-6.51	-0.88	0.17
66.00	-1.34	-3.88	0.58	66.00	-7.32	-0.53	0.29
69.00	-1.60	-3.86	0.43	69.00	-8.31	-0.21	0.42
72.00	-1.87	-3.88	0.25	72.00	-9.53	0.08	0.53
75.00	-2.16	-3.94	0.05	75.00	-11.07	0.33	0.63
78.00	-2.44	-4.04	-0.16	78.00	-13.06	0.53	0.72
81.00	-2.70	-4.19	-0.37	81.00	-15.75	0.69	0.79
84.00	-2.93	-4.37	-0.58	84.00	-19.47	0.80	0.84
87.00	-3.10	-4.59	-0.77	87.00	-23.14	0.86	0.87
90.00	-3.19	-4.84	-0.93	90.00	-20.84	0.86	0.89
93.00	-3.21	-5.12	-1.05	93.00	-16.58	0.82	0.90
96.00	-3.14	-5.41	-1.12	96.00	-13.39	0.72	0.88
99.00	-2.99	-5.71	-1.13	99.00	-11.03	0.57	0.86

102.00	-2.78	-6.00	-1.09	102.00	-9.22	0.36	0.82
105.00	-2.53	-6.26	-0.99	105.00	-7.81	0.11	0.76
108.00	-2.24	-6.47	-0.85	108.00	-6.68	-0.19	0.69
111.00	-1.95	-6.62	-0.68	111.00	-5.79	-0.53	0.60
114.00	-1.66	-6.69	-0.48	114.00	-5.10	-0.89	0.51
117.00	-1.39	-6.67	-0.27	117.00	-4.57	-1.27	0.40
120.00	-1.15	-6.56	-0.05	120.00	-4.18	-1.64	0.28
123.00	-0.94	-6.38	0.15	123.00	-3.91	-1.99	0.16
126.00	-0.77	-6.13	0.34	126.00	-3.76	-2.28	0.05
129.00	-0.64	-5.85	0.50	129.00	-3.72	-2.49	-0.05
132.00	-0.55	-5.54	0.64	132.00	-3.77	-2.59	-0.13
135.00	-0.51	-5.24	0.75	135.00	-3.90	-2.58	-0.18
138.00	-0.50	-4.95	0.83	138.00	-4.12	-2.45	-0.20
141.00	-0.54	-4.68	0.87	141.00	-4.42	-2.23	-0.18
144.00	-0.63	-4.44	0.88	144.00	-4.80	-1.94	-0.13
147.00	-0.75	-4.24	0.86	147.00	-5.27	-1.60	-0.05
150.00	-0.91	-4.08	0.80	150.00	-5.84	-1.24	0.05
153.00	-1.11	-3.97	0.70	153.00	-6.51	-0.88	0.17
156.00	-1.34	-3.90	0.58	156.00	-7.33	-0.53	0.29
159.00	-1.60	-3.87	0.42	159.00	-8.32	-0.21	0.42
162.00	-1.87	-3.89	0.24	162.00	-9.53	0.08	0.53
165.00	-2.16	-3.95	0.05	165.00	-11.07	0.33	0.63
168.00	-2.44	-4.05	-0.16	168.00	-13.06	0.53	0.72
171.00	-2.70	-4.20	-0.38	171.00	-15.75	0.69	0.79
174.00	-2.93	-4.39	-0.59	174.00	-19.48	0.80	0.84
177.00	-3.10	-4.61	-0.78	177.00	-23.19	0.86	0.88
180.00	-3.19	-4.86	-0.94	180.00	-20.87	0.87	0.90
183.00	-3.21	-5.14	-1.06	183.00	-16.60	0.82	0.90
186.00	-3.14	-5.43	-1.13	186.00	-13.40	0.72	0.89
189.00	-2.99	-5.73	-1.14	189.00	-11.03	0.57	0.86
192.00	-2.78	-6.02	-1.10	192.00	-9.22	0.37	0.82
195.00	-2.52	-6.28	-1.00	195.00	-7.81	0.11	0.76
198.00	-2.24	-6.50	-0.86	198.00	-6.68	-0.18	0.69
201.00	-1.95	-6.65	-0.68	201.00	-5.79	-0.52	0.61
204.00	-1.66	-6.71	-0.48	204.00	-5.10	-0.89	0.51
207.00	-1.39	-6.69	-0.27	207.00	-4.56	-1.26	0.40
210.00	-1.15	-6.58	-0.05	210.00	-4.17	-1.64	0.29
213.00	-0.94	-6.39	0.15	213.00	-3.91	-1.98	0.17
216.00	-0.76	-6.15	0.34	216.00	-3.76	-2.27	0.06
219.00	-0.63	-5.86	0.51	219.00	-3.71	-2.47	-0.04
222.00	-0.54	-5.55	0.65	222.00	-3.76	-2.58	-0.12
225.00	-0.50	-5.25	0.76	225.00	-3.90	-2.56	-0.17

228.00	-0.49	-4.95	0.84		228.00	-4.11	-2.44	-0.19
231.00	-0.53	-4.68	0.88		231.00	-4.41	-2.22	-0.17
234.00	-0.62	-4.44	0.89		234.00	-4.80	-1.93	-0.12
237.00	-0.74	-4.24	0.86		237.00	-5.26	-1.59	-0.04
240.00	-0.90	-4.08	0.81		240.00	-5.83	-1.23	0.06
243.00	-1.10	-3.96	0.71		243.00	-6.50	-0.87	0.18
246.00	-1.33	-3.89	0.59		246.00	-7.32	-0.52	0.30
249.00	-1.59	-3.86	0.43		249.00	-8.31	-0.20	0.42
252.00	-1.86	-3.88	0.26		252.00	-9.52	0.09	0.54
255.00	-2.15	-3.94	0.06		255.00	-11.06	0.33	0.64
258.00	-2.43	-4.04	-0.15		258.00	-13.05	0.54	0.72
261.00	-2.69	-4.19	-0.37		261.00	-15.74	0.70	0.79
264.00	-2.92	-4.37	-0.57		264.00	-19.46	0.80	0.84
267.00	-3.09	-4.59	-0.76		267.00	-23.17	0.86	0.88
270.00	-3.19	-4.84	-0.92		270.00	-20.87	0.87	0.90
273.00	-3.20	-5.12	-1.05		273.00	-16.60	0.82	0.90
276.00	-3.14	-5.41	-1.12		276.00	-13.40	0.72	0.89
279.00	-2.99	-5.71	-1.13		279.00	-11.03	0.57	0.86
282.00	-2.79	-5.99	-1.09		282.00	-9.22	0.36	0.82
285.00	-2.53	-6.25	-0.99		285.00	-7.81	0.11	0.76
288.00	-2.25	-6.47	-0.85		288.00	-6.68	-0.19	0.69
291.00	-1.96	-6.62	-0.68		291.00	-5.79	-0.52	0.61
294.00	-1.67	-6.68	-0.48		294.00	-5.09	-0.89	0.51
297.00	-1.40	-6.66	-0.27		297.00	-4.56	-1.27	0.40
300.00	-1.16	-6.56	-0.06		300.00	-4.17	-1.64	0.29
303.00	-0.95	-6.37	0.15		303.00	-3.91	-1.98	0.17
306.00	-0.78	-6.13	0.33		306.00	-3.76	-2.27	0.06
309.00	-0.65	-5.85	0.50		309.00	-3.71	-2.48	-0.04
312.00	-0.56	-5.54	0.64		312.00	-3.75	-2.58	-0.12
315.00	-0.51	-5.24	0.75		315.00	-3.89	-2.57	-0.17
318.00	-0.51	-4.94	0.83		318.00	-4.11	-2.44	-0.19
321.00	-0.55	-4.68	0.87		321.00	-4.41	-2.22	-0.17
324.00	-0.63	-4.44	0.88		324.00	-4.79	-1.93	-0.12
327.00	-0.75	-4.24	0.86		327.00	-5.26	-1.59	-0.04
330.00	-0.91	-4.08	0.80		330.00	-5.82	-1.23	0.06
333.00	-1.11	-3.96	0.70		333.00	-6.49	-0.87	0.18
336.00	-1.34	-3.89	0.58		336.00	-7.31	-0.53	0.30
339.00	-1.60	-3.86	0.43		339.00	-8.29	-0.20	0.42
342.00	-1.87	-3.88	0.25		342.00	-9.51	0.08	0.54
345.00	-2.16	-3.94	0.05		345.00	-11.04	0.33	0.64
348.00	-2.44	-4.04	-0.16		348.00	-13.03	0.54	0.72
351.00	-2.70	-4.19	-0.37		351.00	-15.71	0.69	0.79

354.00	-2.92	-4.37	-0.58		354.00	-19.41	0.80	0.84
357.00	-3.09	-4.59	-0.77		357.00	-23.11	0.86	0.88
360.00	-3.19	-4.84	-0.93		360.00	-20.87	0.87	0.89

**** Power Gains: Phi Pattern ****
Theta=135, Freq=436.5, File=FINAL.DAT

Phi Degrees	Horizontal dB	Vertical dB	Total dB		Phi Degrees	Horizontal dB	Vertical dB	Total dB
0.00	-10.75	-3.64	-2.87		180.00	-10.72	-3.64	-2.86
3.00	-9.95	-3.62	-2.71		183.00	-9.92	-3.63	-2.71
6.00	-9.08	-3.68	-2.58		186.00	-9.06	-3.68	-2.58
9.00	-8.22	-3.80	-2.46		189.00	-8.21	-3.81	-2.46
12.00	-7.43	-3.99	-2.37		192.00	-7.42	-4.00	-2.37
15.00	-6.73	-4.26	-2.31		195.00	-6.71	-4.26	-2.31
18.00	-6.11	-4.59	-2.27		198.00	-6.10	-4.60	-2.27
21.00	-5.59	-4.99	-2.27		201.00	-5.58	-5.00	-2.27
24.00	-5.17	-5.45	-2.30		204.00	-5.16	-5.47	-2.30
27.00	-4.83	-5.98	-2.36		207.00	-4.82	-5.99	-2.36
30.00	-4.58	-6.55	-2.44		210.00	-4.57	-6.57	-2.44
33.00	-4.41	-7.15	-2.56		213.00	-4.40	-7.17	-2.56
36.00	-4.32	-7.74	-2.69		216.00	-4.31	-7.76	-2.70
39.00	-4.31	-8.29	-2.85		219.00	-4.30	-8.31	-2.85
42.00	-4.37	-8.73	-3.02		222.00	-4.37	-8.75	-3.02
45.00	-4.52	-8.99	-3.19		225.00	-4.51	-9.02	-3.19
48.00	-4.73	-9.04	-3.36		228.00	-4.73	-9.06	-3.37
51.00	-5.03	-8.86	-3.53		231.00	-5.03	-8.88	-3.53
54.00	-5.41	-8.48	-3.67		234.00	-5.41	-8.50	-3.68
57.00	-5.87	-7.98	-3.78		237.00	-5.87	-7.99	-3.79
60.00	-6.41	-7.40	-3.87		240.00	-6.41	-7.41	-3.87
63.00	-7.04	-6.80	-3.91		243.00	-7.05	-6.81	-3.91
66.00	-7.75	-6.21	-3.91		246.00	-7.76	-6.22	-3.91
69.00	-8.54	-5.67	-3.86		249.00	-8.55	-5.68	-3.87
72.00	-9.38	-5.18	-3.78		252.00	-9.39	-5.19	-3.79
75.00	-10.21	-4.75	-3.67		255.00	-10.22	-4.76	-3.67
78.00	-10.95	-4.39	-3.53		258.00	-10.96	-4.40	-3.53
81.00	-11.45	-4.10	-3.37		261.00	-11.47	-4.10	-3.37
84.00	-11.60	-3.88	-3.20		264.00	-11.61	-3.88	-3.20
87.00	-11.34	-3.72	-3.03		267.00	-11.35	-3.72	-3.03
90.00	-10.74	-3.64	-2.87		270.00	-10.75	-3.64	-2.87
93.00	-9.94	-3.63	-2.71		273.00	-9.94	-3.62	-2.71
96.00	-9.07	-3.68	-2.58		276.00	-9.07	-3.68	-2.58

46

99.00	-8.22	-3.80	-2.46	279.00	-8.22	-3.80	-2.46
102.00	-7.43	-4.00	-2.37	282.00	-7.43	-3.99	-2.37
105.00	-6.72	-4.26	-2.31	285.00	-6.72	-4.26	-2.31
108.00	-6.11	-4.59	-2.28	288.00	-6.11	-4.59	-2.27
111.00	-5.59	-4.99	-2.27	291.00	-5.59	-4.99	-2.27
114.00	-5.17	-5.46	-2.30	294.00	-5.16	-5.45	-2.30
117.00	-4.83	-5.98	-2.36	297.00	-4.82	-5.98	-2.35
120.00	-4.58	-6.55	-2.44	300.00	-4.57	-6.55	-2.44
123.00	-4.41	-7.15	-2.56	303.00	-4.40	-7.15	-2.55
126.00	-4.32	-7.75	-2.69	306.00	-4.31	-7.74	-2.69
129.00	-4.31	-8.29	-2.85	309.00	-4.30	-8.29	-2.84
132.00	-4.37	-8.73	-3.02	312.00	-4.37	-8.73	-3.01
135.00	-4.52	-8.99	-3.19	315.00	-4.51	-8.99	-3.19
138.00	-4.73	-9.04	-3.36	318.00	-4.73	-9.04	-3.36
141.00	-5.03	-8.85	-3.52	321.00	-5.03	-8.86	-3.52
144.00	-5.41	-8.48	-3.67	324.00	-5.41	-8.48	-3.67
147.00	-5.87	-7.97	-3.78	327.00	-5.87	-7.97	-3.78
150.00	-6.41	-7.39	-3.87	330.00	-6.41	-7.39	-3.86
153.00	-7.04	-6.79	-3.91	333.00	-7.04	-6.79	-3.91
156.00	-7.76	-6.21	-3.91	336.00	-7.76	-6.21	-3.90
159.00	-8.54	-5.67	-3.86	339.00	-8.54	-5.67	-3.86
162.00	-9.38	-5.18	-3.78	342.00	-9.38	-5.18	-3.78
165.00	-10.21	-4.75	-3.67	345.00	-10.22	-4.75	-3.67
168.00	-10.94	-4.39	-3.53	348.00	-10.95	-4.39	-3.53
171.00	-11.45	-4.10	-3.37	351.00	-11.46	-4.10	-3.37
174.00	-11.59	-3.88	-3.20	354.00	-11.61	-3.88	-3.20
177.00	-11.32	-3.73	-3.03	357.00	-11.34	-3.72	-3.03
180.00	-10.72	-3.64	-2.86	360.00	-10.75	-3.64	-2.87

APPENDIX D. MATLAB CODE FOR PLOTTING GAINS

```
%Written by John L. Galenski 111  11/01/93-04/07/94
% All Rights Reserved
function H = polarhg(theta,rho,p1,v1,p2,v2,p3,v3,p4,v4,p5,v5,p6,v6,p7,v7,p8,v8)
%
% POLARHG is similar to polar; however, it is possible to set some
% pseudo-properties.  Below is a table of the pseudo-properties,
% their function, and settings:
%
% PSEUDO-
% PROPERTY   FUNCTION            SETTING/OPTIONS
% --------   --------            --------------
% theta      The theta values    any valid vector
% rho        The rho values      any valid vector
% tdir       Controls the direction  [ClockWise|{CounterClockWise}]
%            that the angles are
%            labeled.
% rlim       Rho limits          NaN -> 2-element vector [min max]
% rtick      Rho tick mark       NaN -> any valid vector
%            location
% tstep      Step used for       30  -> scalar in degrees
%            Drawing the spokes
% torig      Origin of theta     [Up|Down|Left|{Right}]
% color      Color of trace      [RGB Vector|Colorspec|{'Y'}]
% linestyle  Line style          [{-}|+|-|:|.|x|o|*]
%
% Examples of use:
%
% theta = 0:pi/5:pi;
% rho = 10*rand(size(theta));
% h = polarhg(theta,rho,'tdir','clockwise','rlim',[0 10], ...
%         'rtick',[0 3 6 9],'tstep',45,'torig','down', ...
%         'color','m','linestyle',':');
%
% SEE ALSO:  POLAR
%
% LDM052694jlg
%%%%% This M-file has not been tested by the MathWorks, Inc.
%%%%% There are some known problems with error checking,
%%%%% however, the M-file is operational.
%%%%% Note, the grid for the polar plot now consists of two
%%%%% lines.  One connects the spokes, and the other connects
%%%%% the circles.
%%%%% Future enhancements:
%%%%%
%%%%%  ttick      location of spokes
N = nargin;
% Create the property name/property value string arrays
PropFlag = zeros(1,7);
for X = 1:(N-2)/2
 p = eval(['p',int2str(X)]);
 v = eval(['v',int2str(X)]);
 if X == 1
  Property_Names = p;
  Property_Value = v;
 else
  Property_Names = str2mat(Property_Names,p);
  Property_Value = str2mat(Property_Value,v);
 end
 if strcmp(p,'color')
  PropFlag(1) = 1;
  color = v;
 elseif strcmp(p,'rtick')
  PropFlag(2) = 1;
  rtick = v;
 elseif strcmp(p,'rlim')
```

```matlab
    PropFlag(3) = 1;
    rlim = v;
  elseif strcmp(p,'tdir')
    PropFlag(4) = 1;
    tdir = v;
  elseif strcmp(p,'tstep')
    PropFlag(5) = 1;
    tstep = v;
  elseif strcmp(p,'torig')
    PropFlag(6) = 1;
    torig = v;
  elseif strcmp(p,'linestyle')
    PropFlag(7) = 1;
    linestyle = v;
  else
    error(['Invalid pseudo-property name: ',p])
  end
end
% Determine which properties have not been set by
% the user
NotSet = find(PropFlag == 0);
Default_Settings = ['''y''            ';
            'NaN              ';
            'NaN              ';
            '''counterclockwise''  ';
            '30               ';
            '''right''          ';
            '''-''             '];
Property_Names =  ['color   ';
            'rtick   ';
            'rlim    ';
            'tdir    ';
            'tstep   ';
            'torig   ';
            'linestyle'];
for I = 1:length(NotSet)
  eval([Property_Names(NotSet(I),:),'=',Default_Settings(NotSet(I),:),';'])
end
% Start
CurrentAxes = newplot;
NextPlot = get(CurrentAxes,'NextPlot');
HoldFlag = ishold;
AxisColor = get(CurrentAxes,'XColor');
if ~HoldFlag
  hold on
  % make a radial grid
  if ~isnan(rlim)            % rlim is defined
    MinRho = find(rho<min(rlim));  % Minimum rho limit
    MaxRho = find(rho>max(rlim));   % Maximum rho limit
    rho([MinRho,MaxRho]) = [].*ones(size([MinRho,MaxRho]));
    theta([MinRho,MaxRho]) = [].*ones(size([MinRho,MaxRho]));
  end
  Temp=plot([0 max(theta(:))],[0 max(abs(rho(:)))]); % Initialize plotting info
  AxisLim = [get(CurrentAxes,'xlim') get(CurrentAxes,'ylim')];
  NumTicks = length(get(CurrentAxes,'ytick'));
  delete(Temp);
  % check radial limits and ticks
  if isnan(rtick)          % rtick not defined
    if ~isnan(rlim)         % rlim is defined
      Rmin = rlim(1);       % Initialize Rmin
      Rmax = rlim(2);       % Initialize Rmax
    else              % rlim is not defined
      Rmin = 0;           % Set Rmin = 0
      Rmax = AxisLim(4);      % Set Rmax = maximum y-axis value
    end
    NumTicks = NumTicks-1;      % Number of circles
    if NumTicks > 5         % see if we can reduce the number
      if rem(NumTicks,2) == 0
```

49

```
      NumTicks = NumTicks/2;
    elseif rem(NumTicks,3) == 0
      NumTicks = NumTicks/3;
    end
  end
  Rinc = (Rmax-Rmin)/NumTicks;    % Distance between circles
  rtick = (Rmin+Rinc):Rinc:Rmax;  % radii of circles
else                   % rtick is defined
  if isnan(rlim)           % rlim is not defined
    Rmin = 0;              % set Rmin = 0
    Rmax = max(rtick);         % set Rmax = max rtick value
  else                  % rlim is defined
    Rmin = min(rlim);         % set Rmin = minimum rlim
    Rmax = max(rlim);          % set Rmax = maximum rlim
    RtickMin = find(rtick<Rmin); % find elements of rtick < min(rlim)
    RtickMax = find(rtick>Rmax); % find elements of rtick > max(rlim)
                   % remove these values from rtick
    rtick([RtickMin,RtickMax]) = [].*ones(size([RtickMin,RtickMax]));
  end
  rtick = [Rmin,rtick,Rmax];      % the new radii
  set(CurrentAxes,'Ylim',[Rmin Rmax]) % set the Y-limits to [Rmin Rmax]
  NumTicks = length(rtick)-1;    % number of circles
end
% plot spokes
th = (1:.5*360/tstep)*2*pi*tstep/360; % define the spokes
cst = cos(th);
snt = sin(th);
cs = [-cst; cst];
sn = [-snt; snt];
cs = [cs;NaN.*cs(1,:)];
sn = [sn;NaN.*sn(1,:)];
% plot the spokes
hh = plot((Rmax-Rmin)*cs(:),(Rmax-Rmin)*sn(:),'-', ...
        'color',AxisColor,'linewidth',1);
set(0,'UserData',hh)
% annotate spokes in degrees
Rt = 1.1*(Rmax-Rmin);
for i = 1:max(size(th))
  text(Rt*cst(i),Rt*snt(i),int2str(i*tstep),'horizontalalignment','center');
  if i == max(size(th))
    loc = int2str(0);
  else
    loc = int2str(180+i*tstep);
  end
  text(-Rt*cst(i),-Rt*snt(i),loc,'horizontalalignment','center');
end
% set view to 2-D.  Use the appropriate view (tdir)
tdir = lower(tdir);
torig = lower(torig);
if strcmp(tdir(1:5),'count') & strcmp(torig,'right')
  view(0,90);
  InitTh = 0;
elseif strcmp(tdir(1:5),'count') & strcmp(torig,'left')
  view(180,90);
  InitTh = 1;
elseif strcmp(tdir(1:5),'count') & strcmp(torig,'up')
  view(-90,90);
  InitTh = 2;
elseif strcmp(tdir(1:5),'count') & strcmp(torig,'down')
  view(90,90);
  InitTh = 3;
elseif strcmp(tdir(1:5),'clock') & strcmp(torig,'right')
  view(0,-90);
  InitTh = 0;
elseif strcmp(tdir(1:5),'clock') & strcmp(torig,'left')
  view(180,-90);
  lnitTh = 1;
elseif strcmp(tdir(1:5),'clock') & strcmp(torig,'up')
```

```
    view(90,-90);
    InitTh = 2;
  elseif strcmp(tdir(1:5),'clock') & strcmp(torig,'down')
    view(-90,-90);
    InitTh = 3;
  else
    error('Invalid TDir or TOrig')
  end
  if strcmp(torig,'up') | strcmp(torig,'down')
    axis square
  end
  % define a circle
  th = 0:pi/75:2*pi;
  xunit = cos(th);
  yunit = sin(th);
  % This code has been vectorized so that only one line
  % is used to draw the circles.
  MultFact = rtick-Rmin;
  [MM,NN] = size(MultFact);
  [MMM,NNN] = size(xunit);
  XUNIT = [MultFact' * ones(1,NNN)] .* [ones(NN,1) * xunit];
  YUNIT = [MultFact' * ones(1,NNN)] .* [ones(NN,1) * yunit];
  XUNIT = XUNIT';
  YUNIT = YUNIT';
  XX = [XUNIT;NaN.*XUNIT(I,:)];
  YY = [YUNIT;NaN.*YUNIT(I,:)];
  hhh = plot(XX(:),YY(:),'-','Color',AxisColor,'LineWidth',I);
  % Add the text and make sure that it always starts at the origin
  % and moves up.
  for i = MultFact
    if InitTh == 0       % Right
      Xt = 0;
      Yt = i;
    elseif InitTh == 1   % Left
      Xt = 0;
      Yt = -i;
    elseif InitTh == 2   % Up
      Xt = i;
      Yt = 0;
    elseif InitTh == 3   % Down
      Xt = -i;
      Yt = 0;
    else
      Xt = 0;
      Yt = i;
    end
    text(Xt,Yt,num2str(i+Rmin),'VerticalAlignment','bottom', ...
        'HorizontalAlignment','left');
  end
  % set axis limits
  axis((Rmax-Rmin)*[-1 1 -1.I 1.1]);
end
% transform data to Cartesian coordinates.
xx = (rho-Rmin).*cos(theta); % I'm not sure if this is correct
yy = (rho-Rmin).*sin(theta);
% plot data on top of grid
q = plot(xx,yy);
set(q,'Color',color,'linestyle',linestyle)
if nargout > 0
    hpol = q;
end
if ~HoldFlag
    axis('equal');axis('off');
end
% reset hold state
if ~HoldFlag, set(CurrentAxes,'NextPlot',NextPlot); end
```

APPENDIX E. PROGRAM TO INPUT DATA TO PLOTTING ROUTINE

```
% Written by Gary Smilowitz May 1997
function y = drawme(data);


angles=data(:,2);
value_H_low=data(:,4);
value_H_level=data(:,6);
value_H_high=data(:,8);
value_V_low=data(:,3);
value_V_level=data(:,5);
value_V_high=data(:,7);
Vert = [data(:,3),data(:,5),data(:,7)];
Horiz = [data(:,4),data(:,6),data(:,8)];

[Y,I] = min(Vert);
min_V=min(Y);
[Y,I] = min(Horiz);
min_H=min(Y);

[Y,I] = max(Vert);
max_V=max(Y);
[Y,I] = max(Horiz);
max_H=max(Y);

rlim_h=[min_H,max_H];
rlim_v=[min_V,max_V];
rlim_tot = [-40,5];
%rlim_tot = [min(min_H,min_V),max(max_H,max_V)];



polarhg(angles,value_H_low,'color','k','linestyle','*','rlim',rlim_tot,'rtick',[-5,-10,-15,-20,-25]);
title('Theta = 135 Horizontal Low');

figure(2)
polarhg(angles,value_H_level,'color','k','linestyle','x','rlim',rlim_tot,'rtick',[-5,-10,-15,-20,-25])
title('Theta = 135 Horizontal Level');

figure(3)
polarhg(angles,value_H_high,'color','k','linestyle','*','rlim',rlim_tot,'rtick',[-5,-10,-15,-20,-25])
title('Theta = 135 Horizontal High');

figure(4);
polarhg(angles,value_V_low,'color','k','linestyle','*','rlim',rlim_tot,'rtick',[-5,-10,-15,-20,-25]);
title('Theta = 135 Vertical Low');

figure(5)
polarhg(angles,value_V_level,'color','k','linestyle','x','rlim',rlim_tot,'rtick',[-5,-10,-15,-20,-25])
title('Theta = 135 Vertical Level');

figure(6)
polarhg(angles,value_V_high,'color','k','linestyle','*','rlim',rlim_tot,'rtick',[-5,-10,-15,-20,-25])
title('Theta = 135 Vertical High');
```

APPENDIX F. MATLAB AND NEC PLOTS OF FIELD TESTS
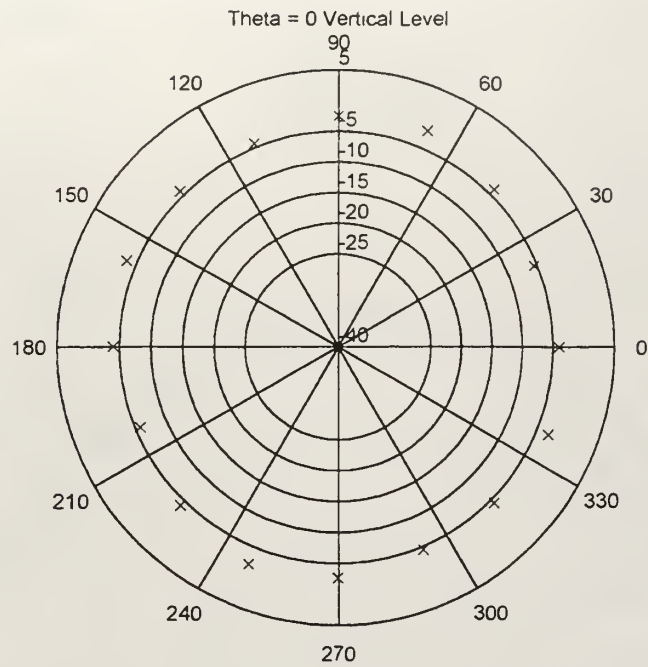
Figure 26 Field Test (Vertical, $\theta_{sat}=0^o$)
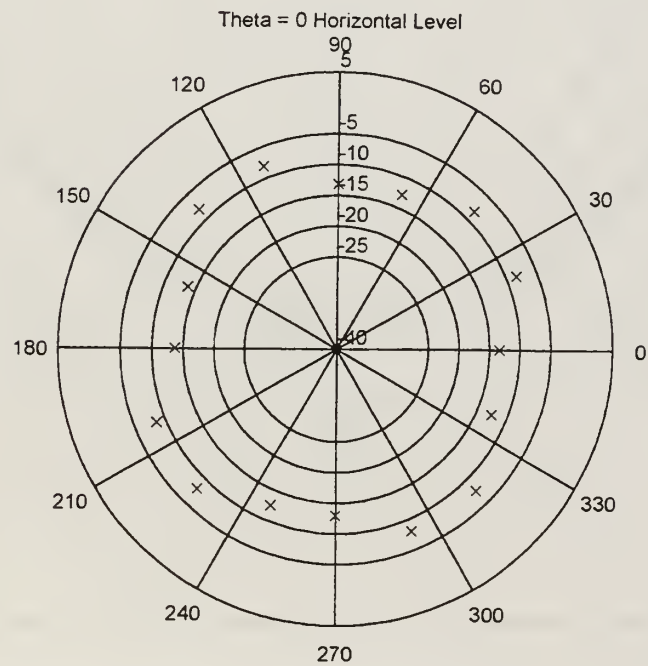
Figure 27 Field Test (Horizontal, $\theta_{sat}=0^o$)

53
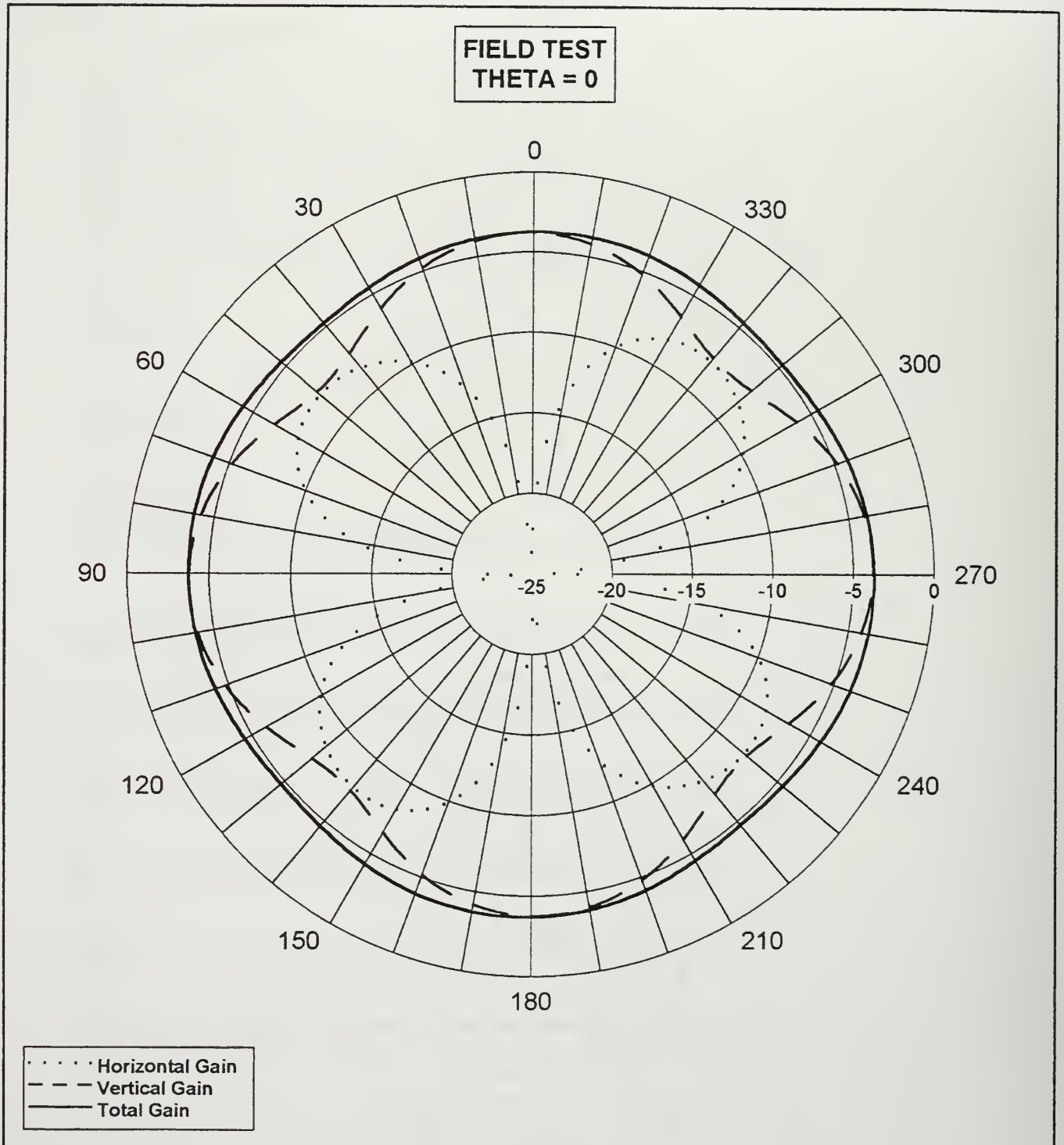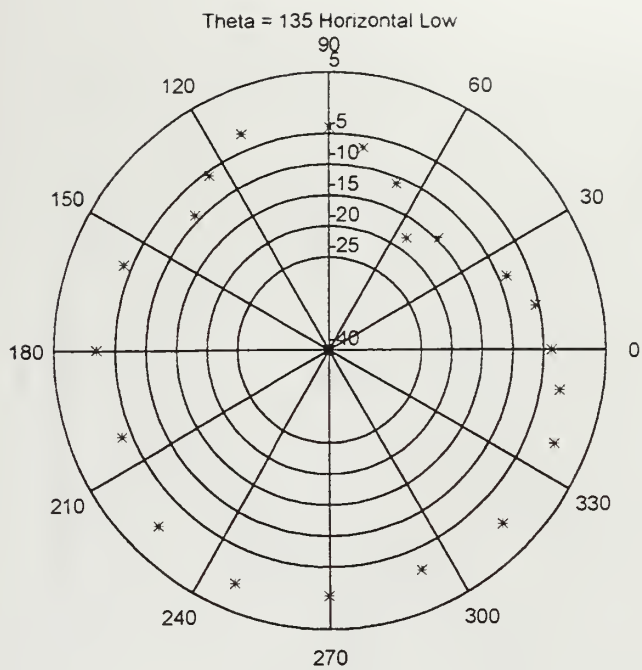
Figure 28 NEC Plot of Field Test ($\theta_{sat}=0^{o}$)
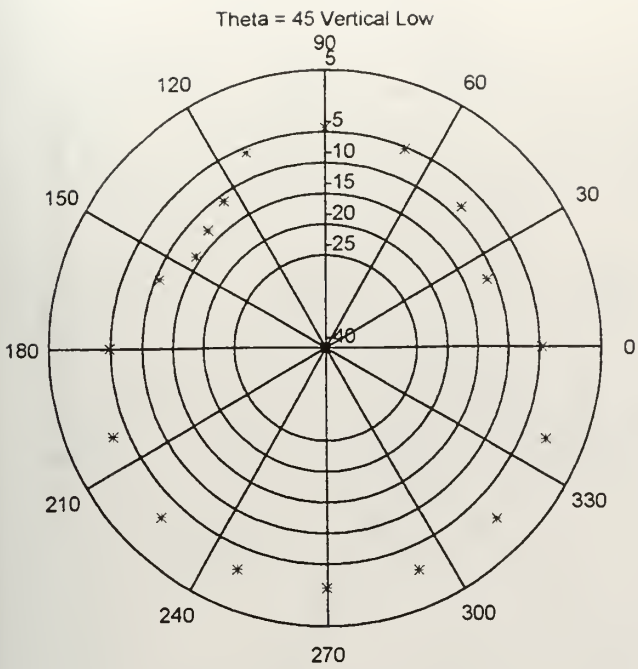
Figure 29 Field Test-Low
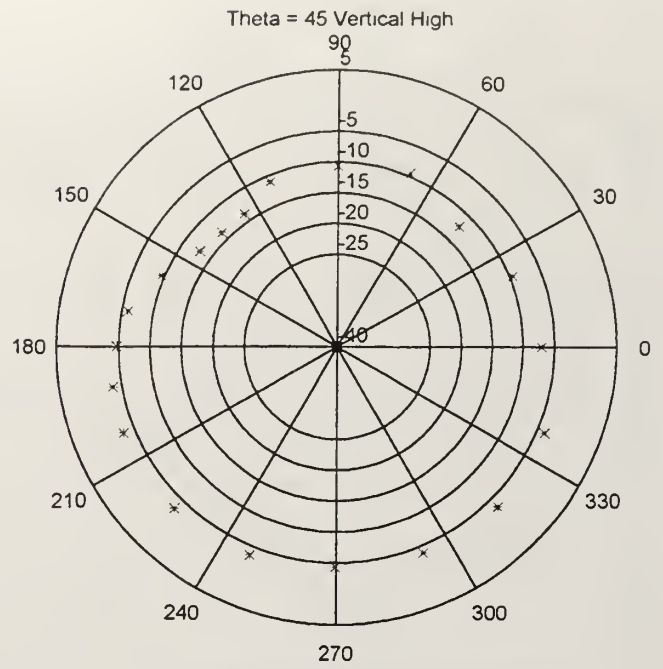
Figure 30 Field Test-High
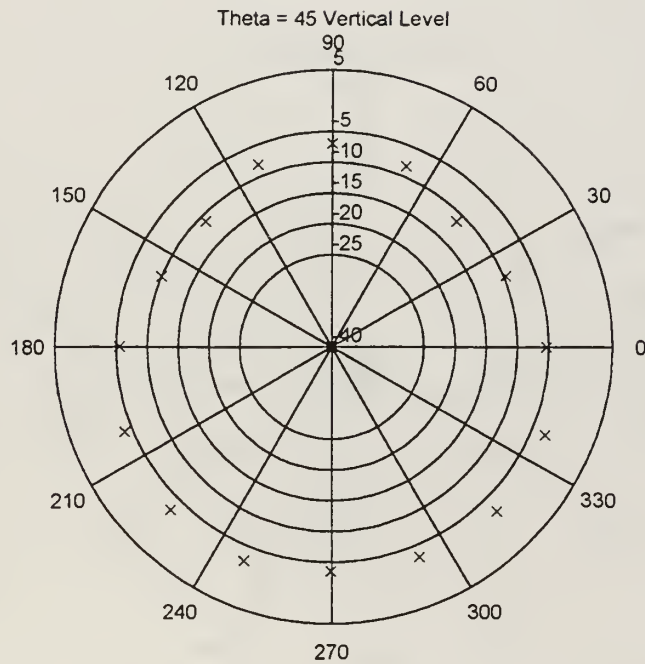
Figure 31 Field Test-Level (Vertical, $\theta_{sat}=45^o$)

Figure 32 Field Test-Low
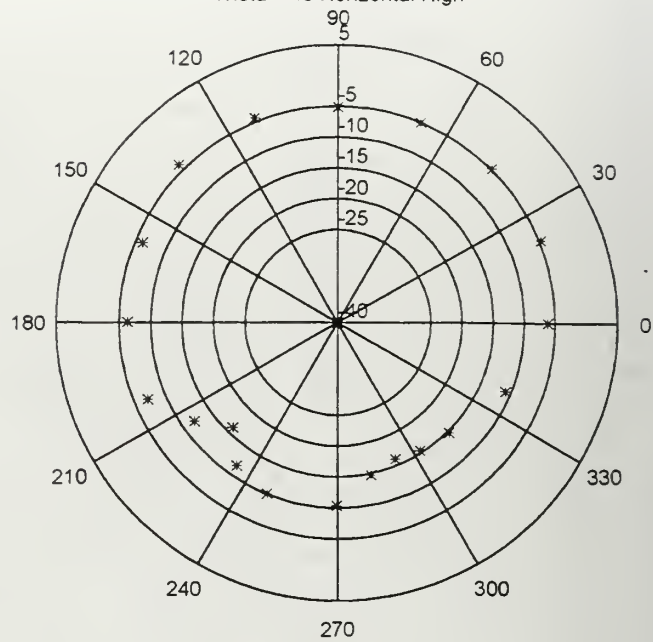
Figure 33 Field Test-High

*Figure 34 Field Test-Level (Horizontal, $\theta_{sat}=45^o$)*

56
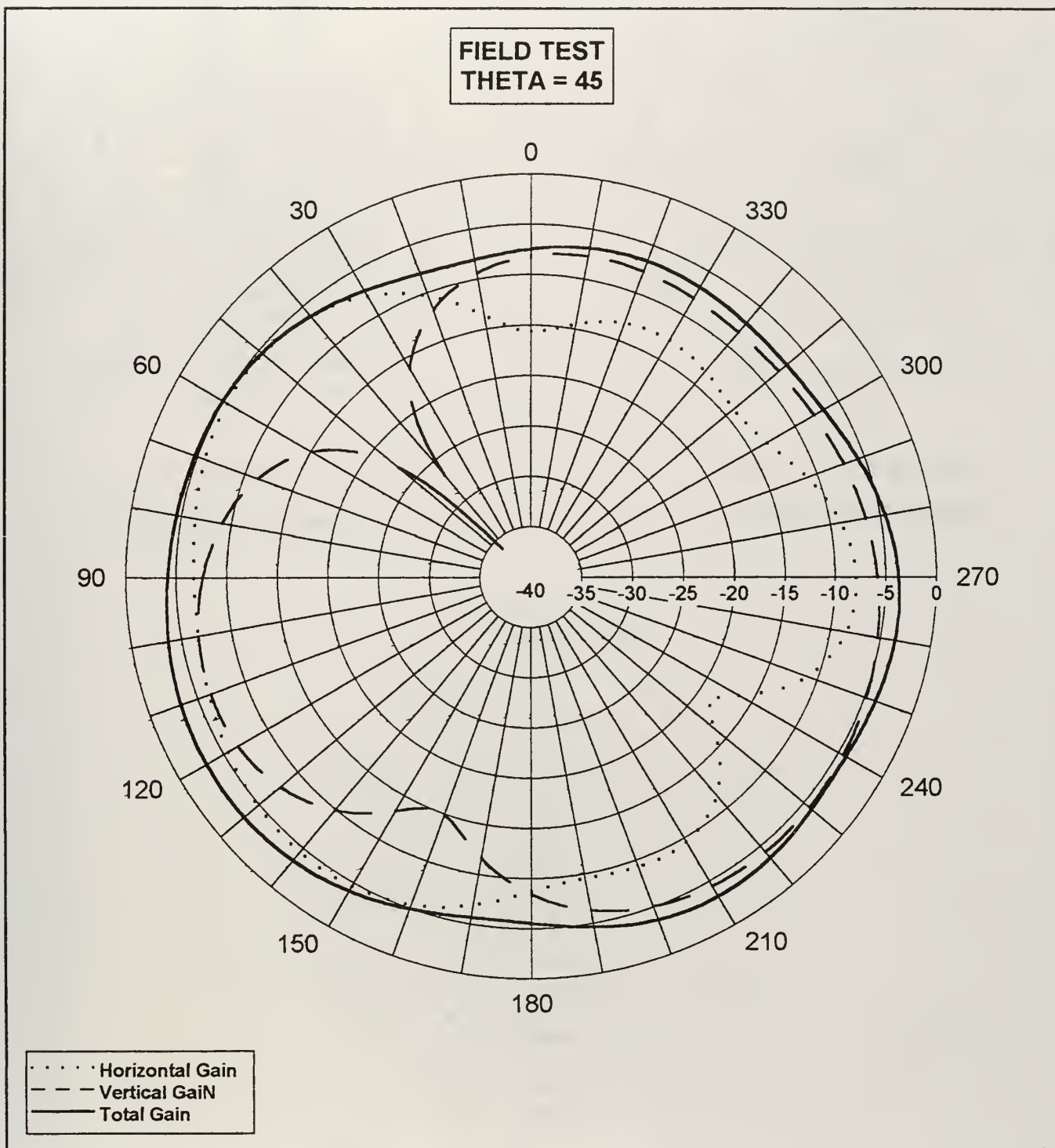
Figure 35 NEC Plot of Field Test ($\theta_{sat}=45^o$)
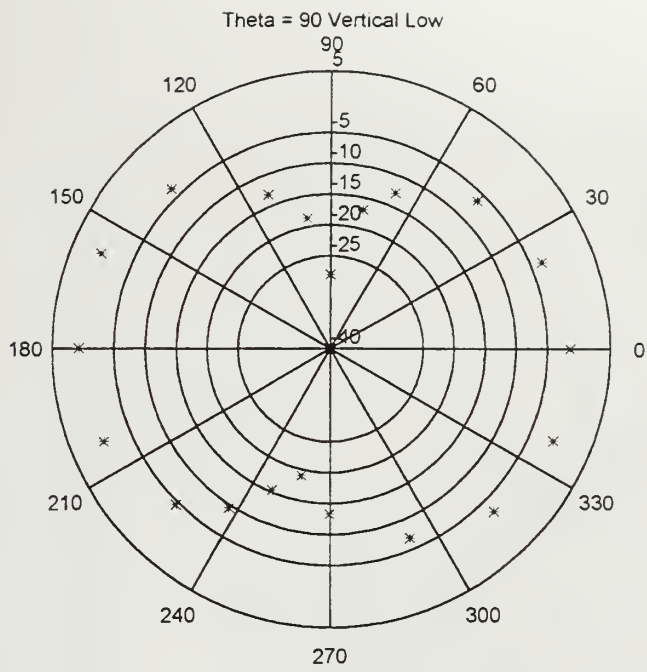
Figure 36 Field Test-Low
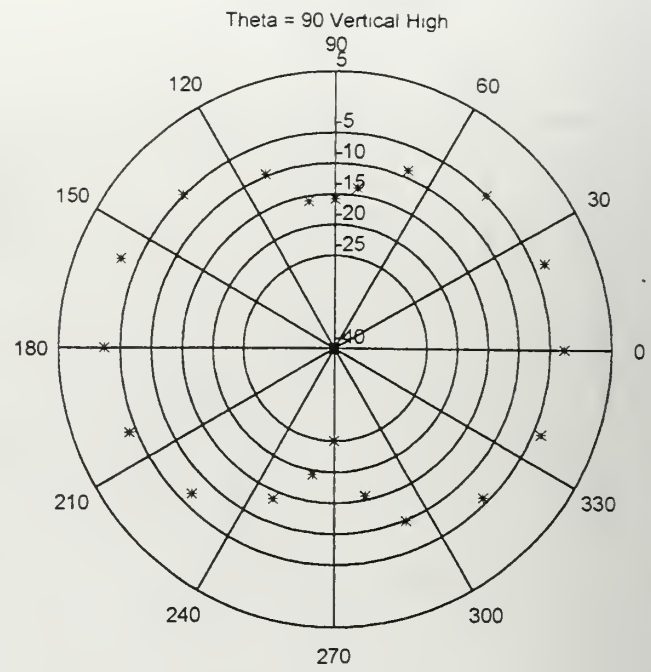
Figure 37 Field Test-High
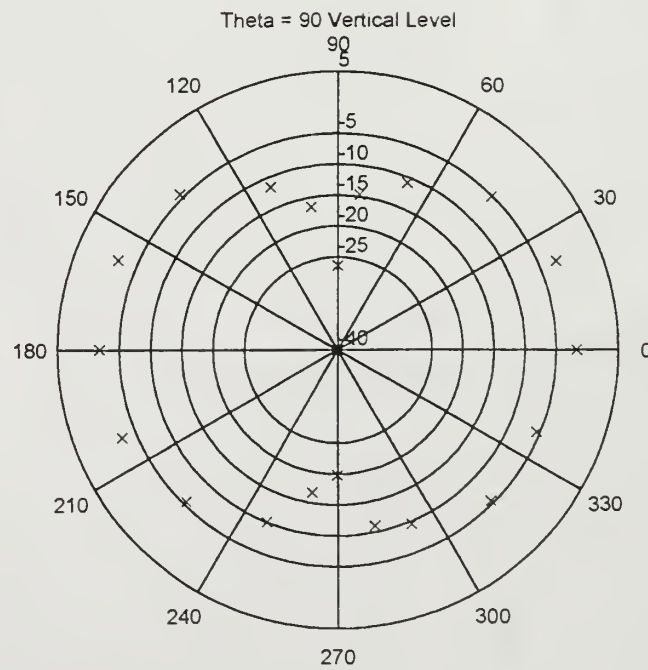
Figure 38 Field Test-Level (Vertical , $\theta_{sat}=90^o$)

58

Figure 39 Field Test-Low
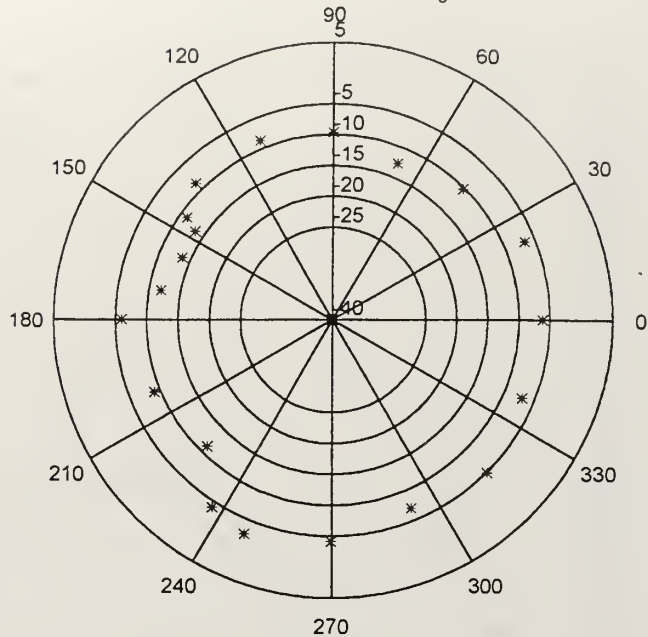
Figure 40 Field Test-High
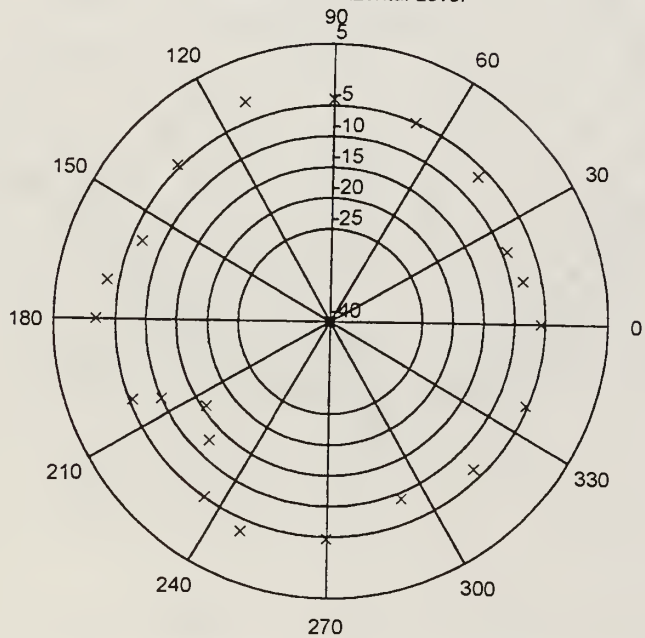
Figure 41 Field Test-Level (Horizontal, $\theta_{sat}=90^{o}$)

59
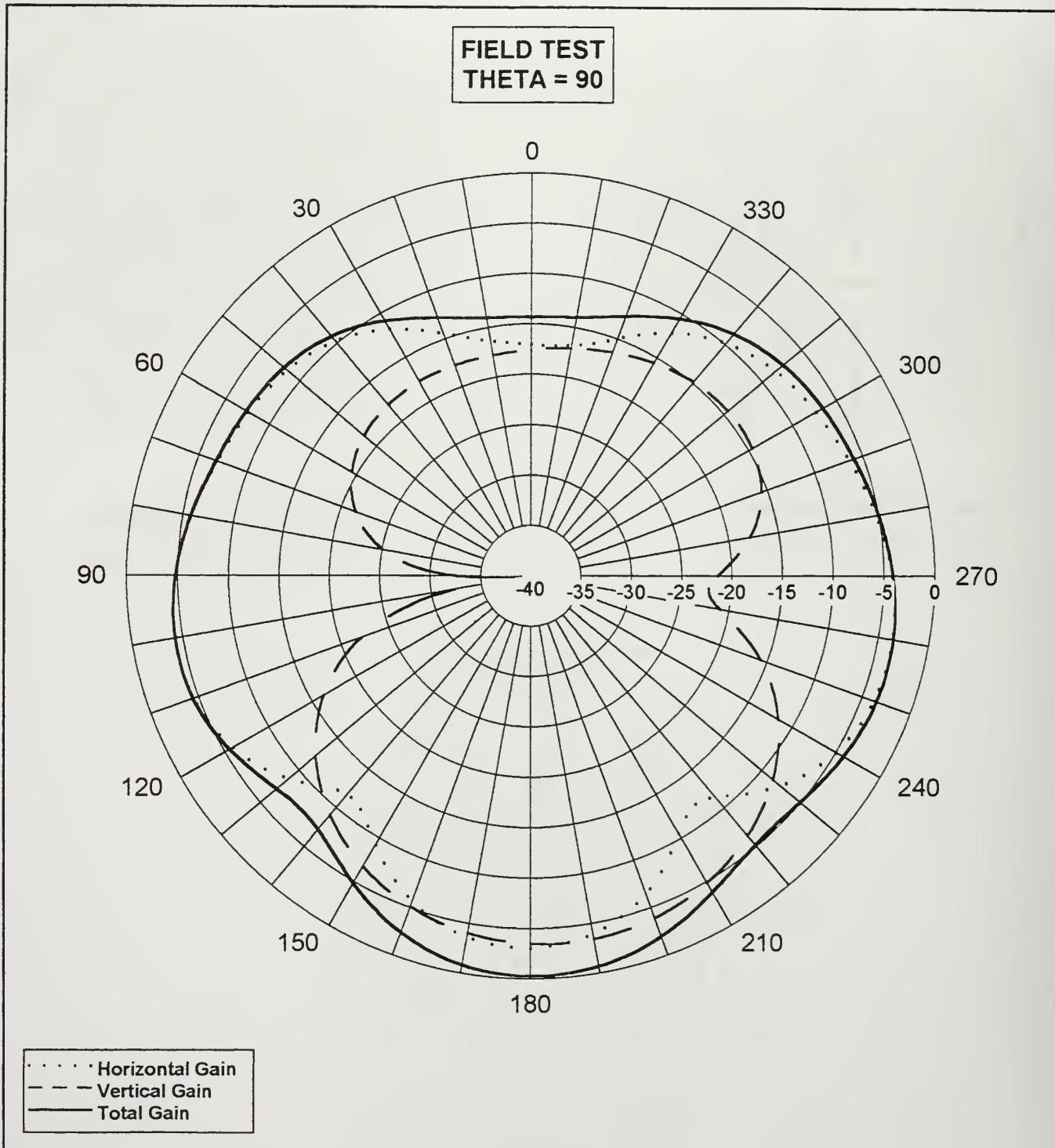
Figure 42 NEC Plot of Field Test ($\theta_{sat}=90^{o}$)
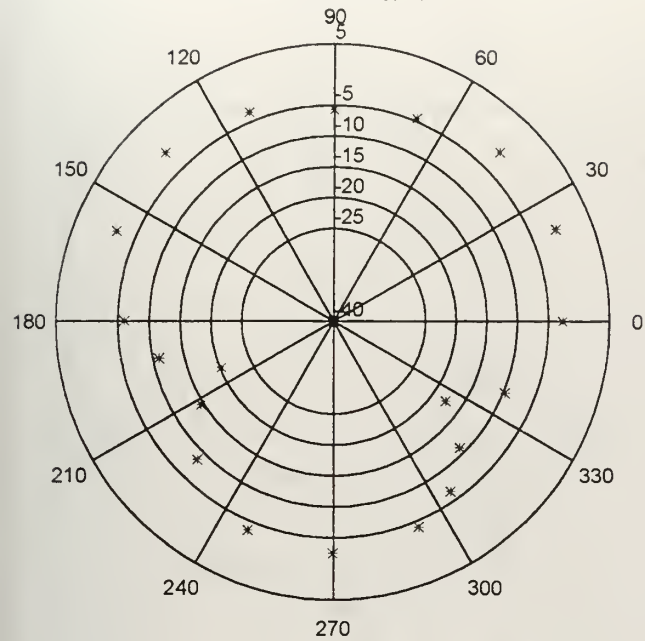
Figure 43 Field Test-Low

Figure 44 Field Test-High

Figure 45 Field Test-Level (Vertical , $\theta_{sat}=135^o$)

61

Figure 46 Field Test-Low
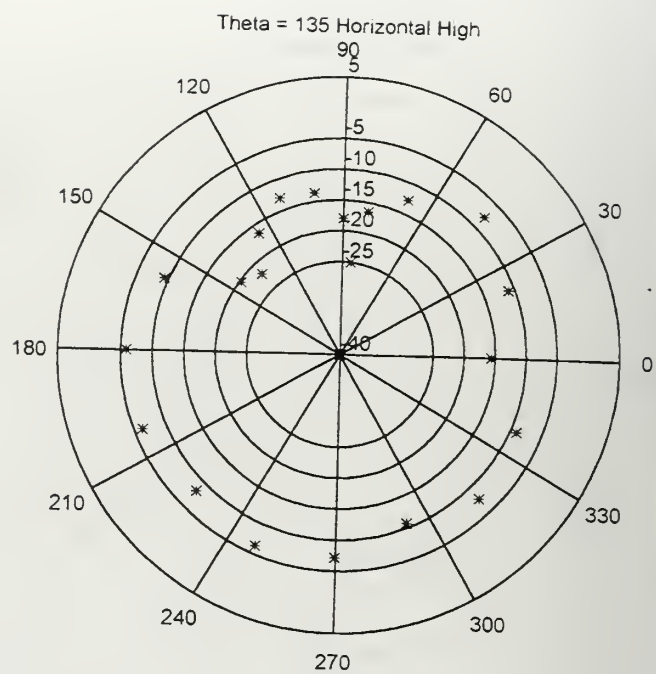
Figure 47 Field Test-High
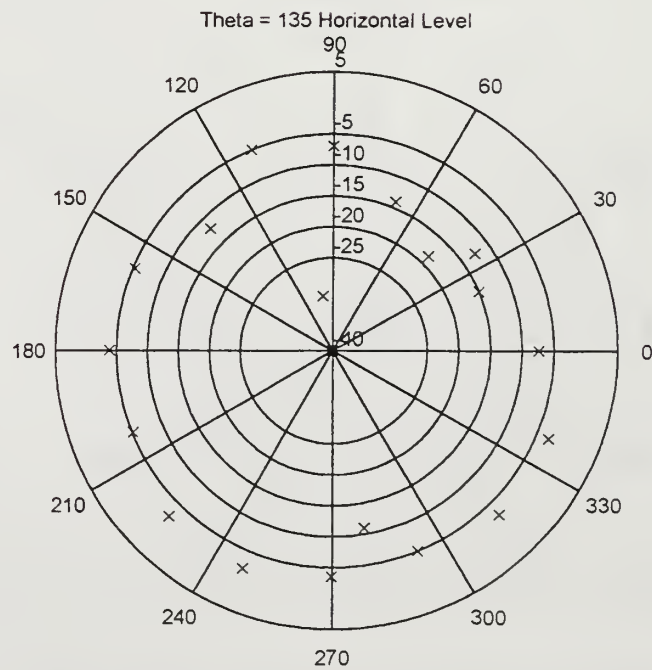
Figure 48 Field Test-Level (Horizontal, $\theta_{sat}=135^{o}$)
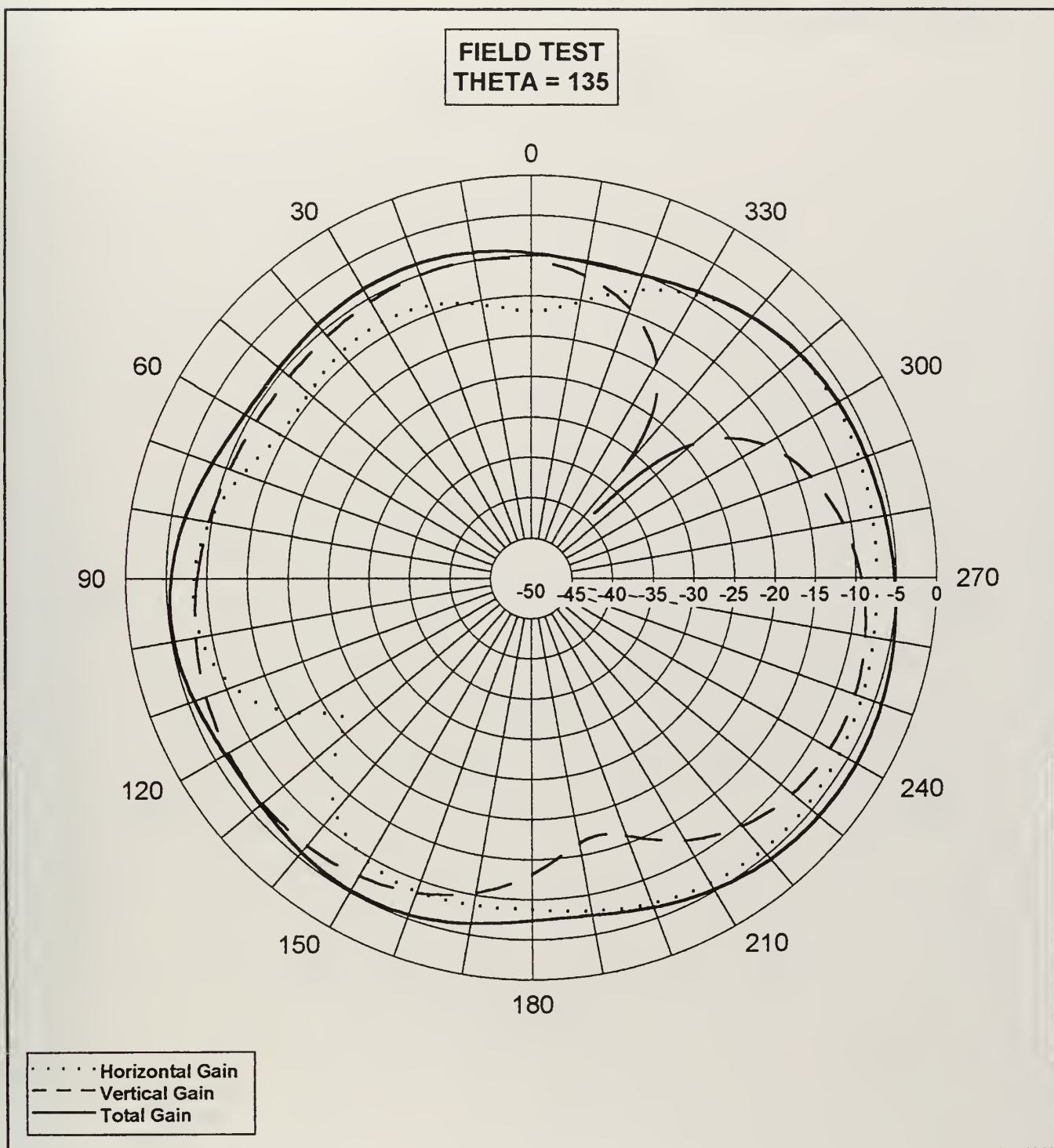
Figure 49 NEC Plot of Field Test ($\theta_{sat}=135^{o}$)

APPENDIX G. GROUND STATION REFERENCE SECTION

This section will provide the ground station with the final plots of the power gains for the NEC free-space model.

1.   GAIN PATTERN FOR $\Theta_{SAT} = 0^O$, $\Phi_{SAT}=45^O$
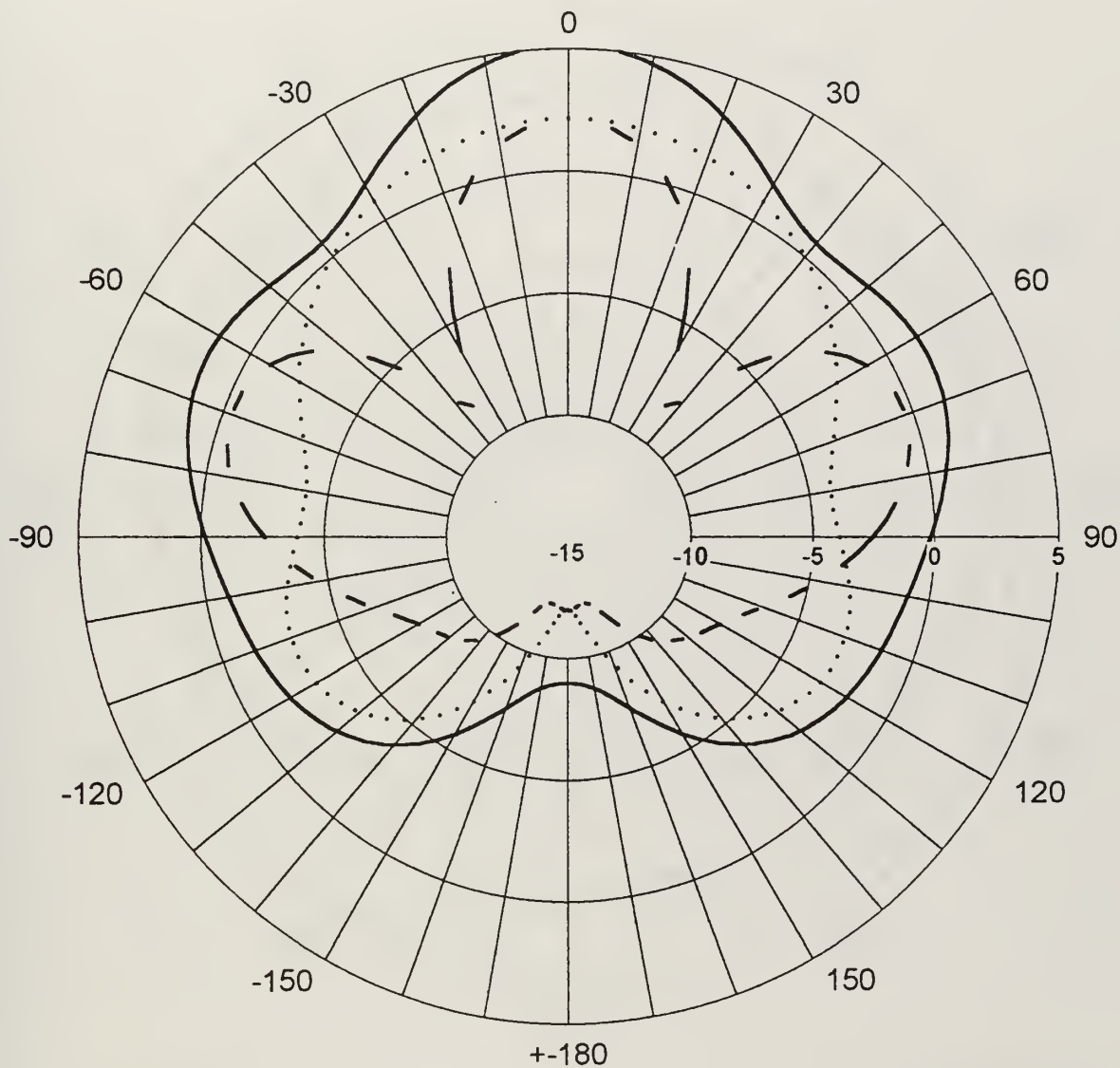
Figure 50 Power Gain Pattern ($\theta_{sat} = 0^o$, $\phi_{sat}=45^o$)

2.   GAIN PATTERN FOR $\Theta_{SAT} = 0^O$, $\Phi_{SAT} = 90^O$
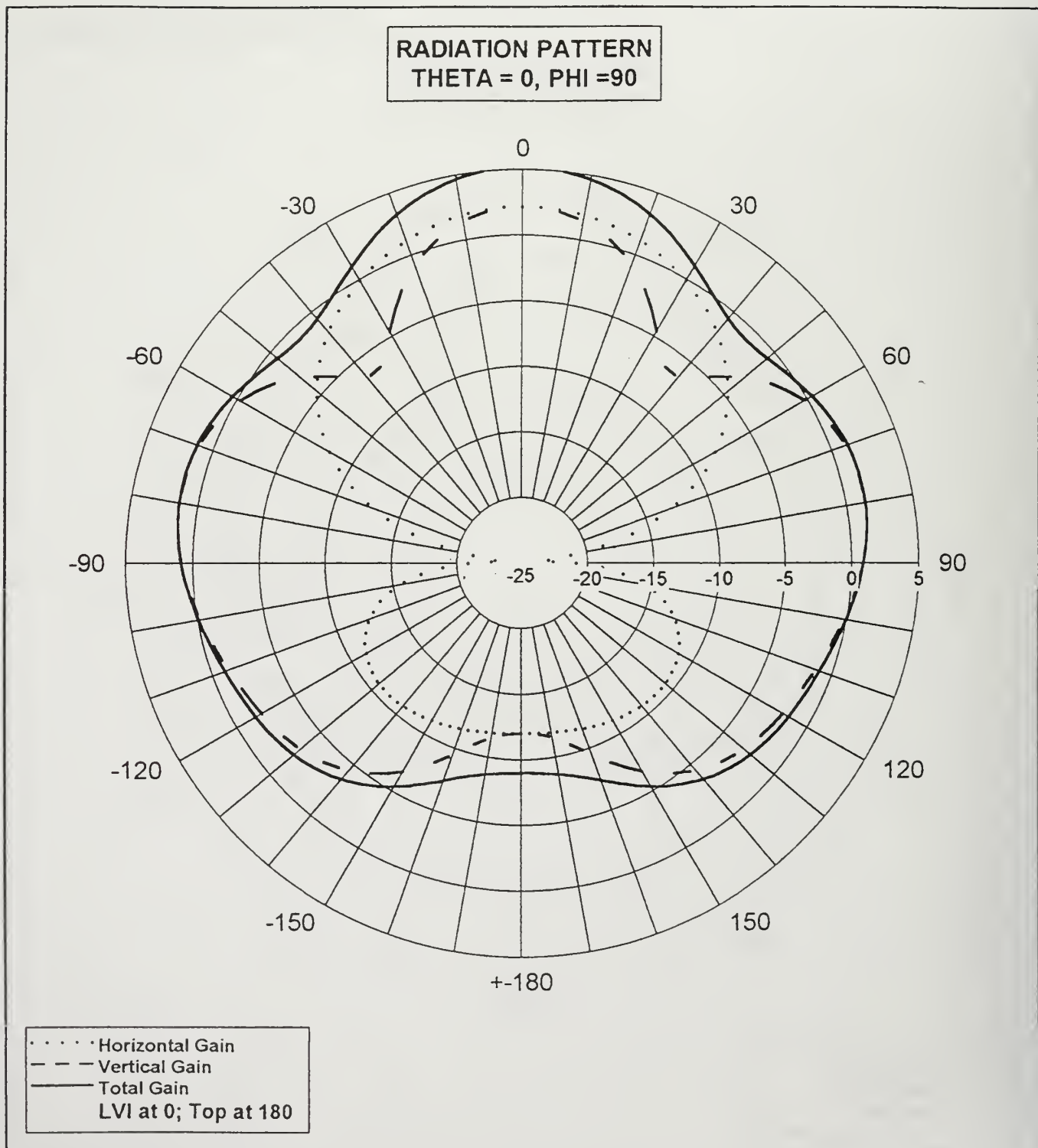
Figure 51 Power Gain Pattern ($\theta_{sat} = 0^o$, $\phi_{sat} = 90^o$)
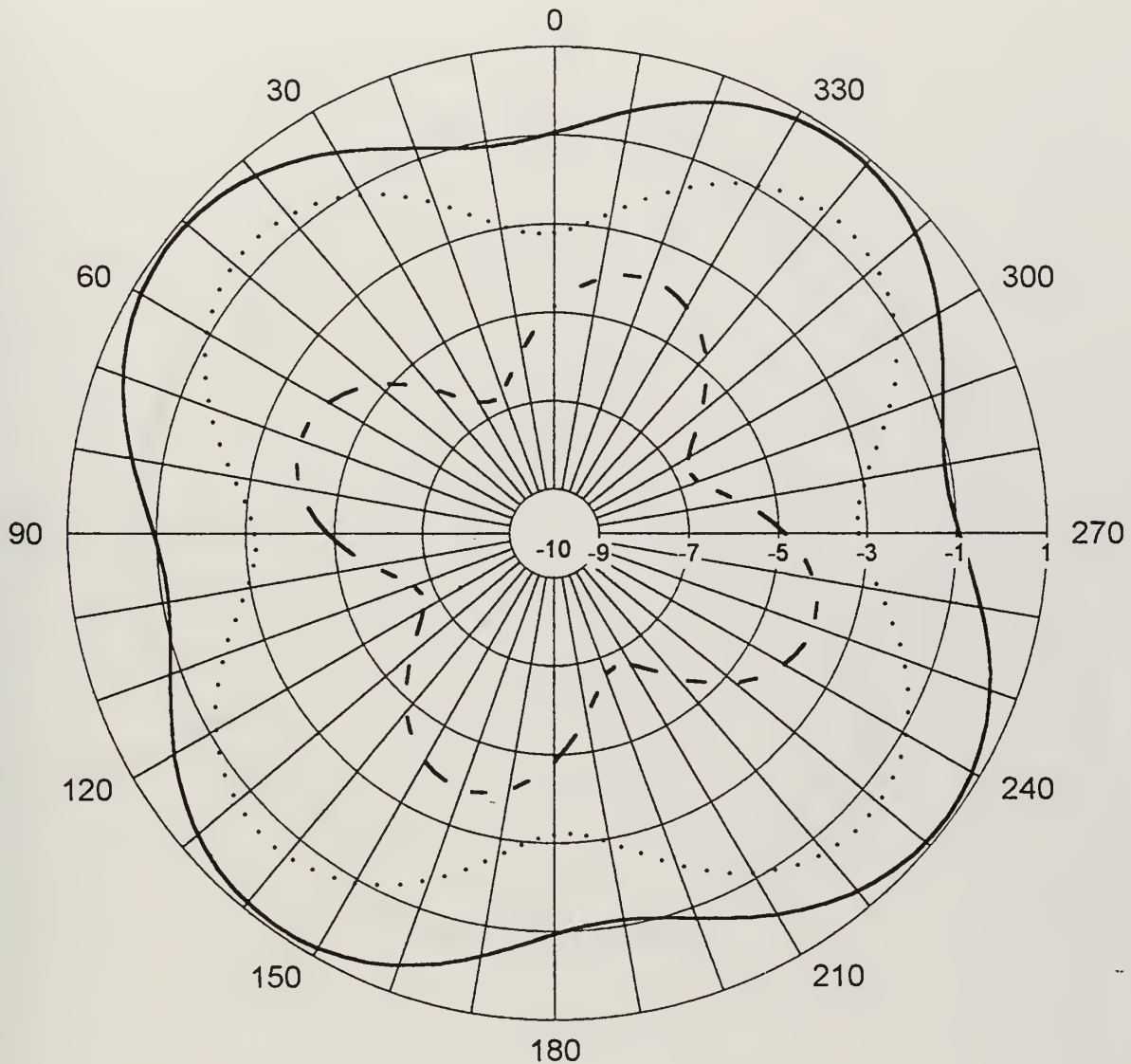
Figure 52 Power Gain Pattern ($\theta_{sat} = 45^o$)

4. GAIN PATTERN FOR $\Theta_{SAT} = 90^O$
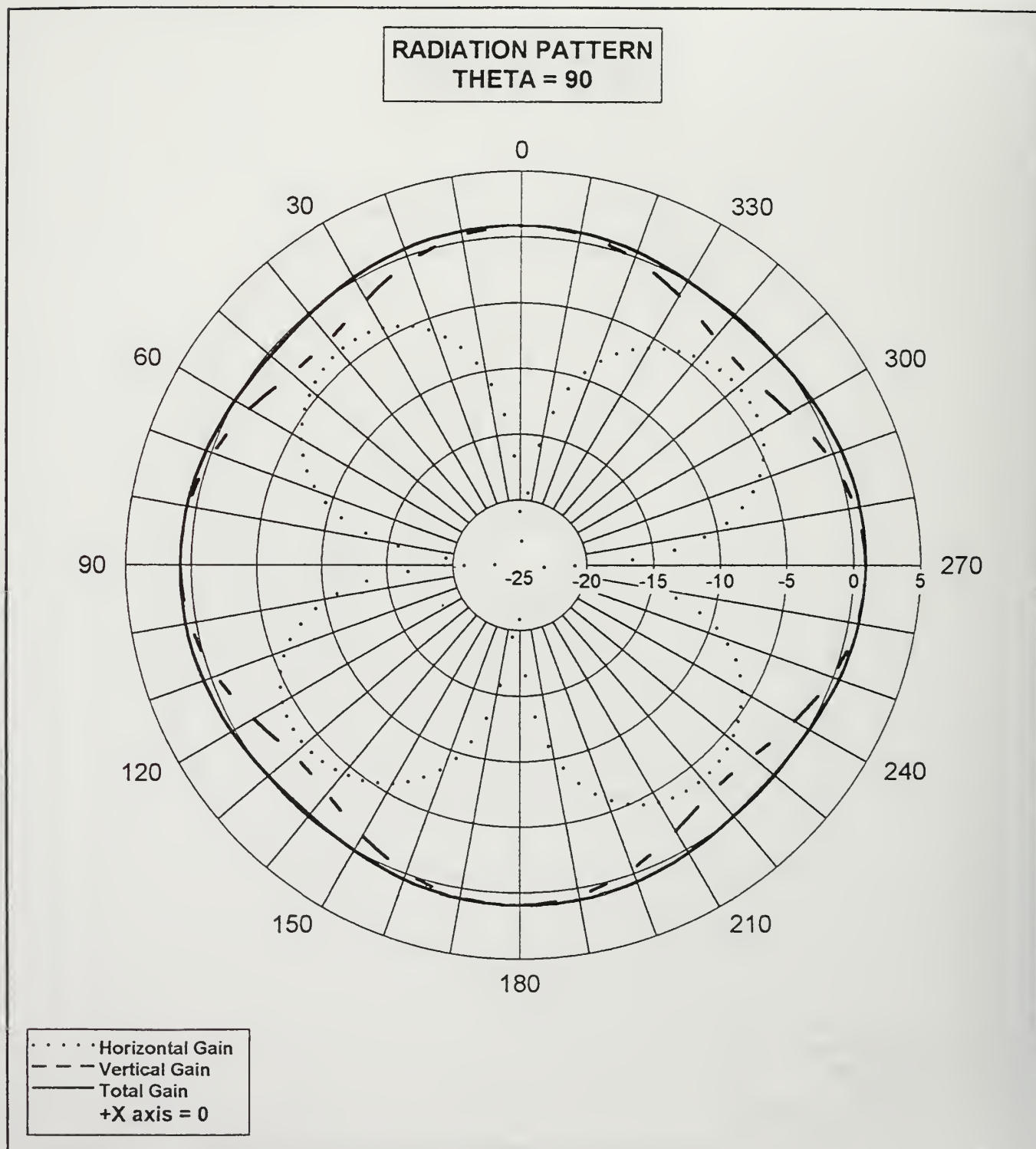
Figure 53 Power Gain Pattern($\theta_{sat} = 90^o$)

5. GAIN PATTERN FOR $\Theta_{SAT} = 135^O$
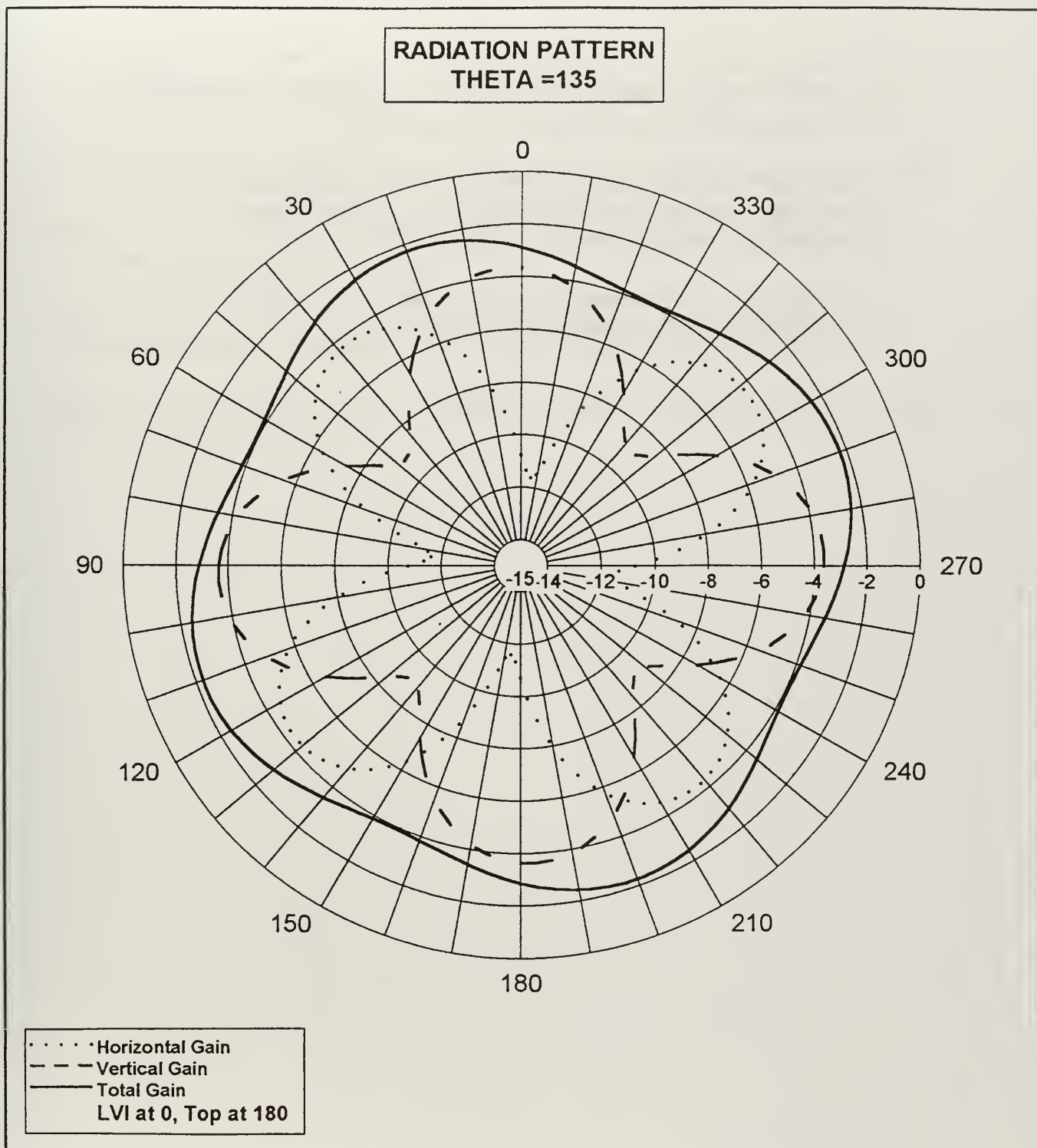
Figure 54 Power Gain Pattern ($\theta_{sat} = 135^o$)

LIST OF REFERENCES

1. D. A. Ellrick, "An Antenna Design for PANSAT Using NEC, " Master's Thesis, Naval Postgraduate School, Monterey, CA., June 1991.

2. E. Karapinar, " Modification and Verification of an Antenna Design for the Petite Amateur Navy Satellite (PANSAT) Using NEC, " Master's Thesis, Naval Postgraduate School, Monterey, CA., June 1995.

3. R. P. W. King , C. W. Harrison , Jr., *Antennas and Waves, A Modern Approach*, The MIT Press, Cambridge, MA, 1983.

BIBLIOGRAPHY

Albertson, N. C., Hansen, J. E., and Jensen, N. E. "Numerical Prediction of Radiation Patterns for Antennas Mounted on Spacecraft, " *IEEE Conference Publication*, no. 77, p.219, June 1971.

Elliot, R. S., *Antenna Theory and Design*, Prentice Hall, Inc., Englewood Cliffs, NJ, 1981

Johnk, C. T. A., *Engineering Electromagnetic Fields and Waves*, John Wiley and Sons, Inc., New York, NY, 1975.

King, R. P. W., Smith, G. S., with Owens, M., Wu T. T., *Antennas in Matter Fundamentals, Theory and Applications*, The MIT Press, Cambridge MA, 1981.

King, R. P. W., Harrison, C. W., Jr., *Antennas and Waves, A Modern Approach*, The MIT Press, Cambridge, MA, 1983.

INITIAL DISTRIBUTION LIST